# Correction of Conductance Measurements in Non-Space-Clamped Structures: 1. Voltage-Gated $K^+$ Channels

Andreas T. Schaefer,* Moritz Helmstaedter,* Bert Sakmann,* and Alon Korngreen*†
*Abteilung Zellphysiologie, Max-Planck-Institut für medizinische Forschung, D-69120 Heidelberg, Germany; and
†Faculty of Life Sciences, Bar-Ilan University, Ramat-Gan 52900, Israel

ABSTRACT To understand functions of a single neuron, such as propagation and generation of synaptic or action potentials, a detailed description of the kinetics and distribution of the underlying ionic conductances is essential. In voltage-clamp experiments, incomplete space clamp distorts the recorded currents, rendering accurate analysis impossible. Here, we present a simple numerical algorithm that corrects such distortions. The method performs a stepwise approximation of the conductance density at the site of a local voltage clamp. This is achieved by estimating membrane conductances in a simulation that yields simulated clamp currents, which are then fitted to the distorted recordings from the non-space-clamped structure, relying on accurately reconstructed cell morphology and experimentally determined passive properties. The method enabled accurate retrieval of the local densities, kinetics, and density gradients of somatic and dendritic channels. Neither the addition of noise nor variation of passive parameters significantly reduced the performance of the correction algorithm. The correction method was applied to two-electrode voltage-clamp recordings of $K^+$ currents from the apical dendrite of layer 5 neocortical pyramidal neurons. The generality and robustness of the algorithm make it a useful tool for voltage-clamp analysis of voltage-gated currents in structures of any morphology that is amenable to the voltage-clamp technique.

## INTRODUCTION

Understanding the function of a single neuron requires quantitative description of the ionic channels it expresses. Such a description is usually achieved using the voltage-clamp technique (Hodgkin and Huxley, 1952). However, voltage-clamp recordings can only be properly analyzed in isopotential structures. Problems that occur upon incomplete space clamp have been addressed extensively (Armstrong and Gilly, 1992; Augustine et al., 1985; Johnston et al., 1996; Koch, 1999; Larsson et al., 1997; Major, 1993; Major et al., 1993; Müller and Lux, 1993; Rall et al., 1992; Rall and Segev, 1985; Spruston et al., 1993; White et al., 1995). Typically, voltage-clamp recordings from neurons are severely distorted, which makes it impossible to directly determine properties of ionic conductances, even for small neurons. So far, only a few theoretical and experimental techniques enable true voltage-clamp recordings from specific branched structures either by analytical transformations (Cole and Curtis, 1941), or by recording conditions (Adrian et al., 1970; Augustine et al., 1985). Currently available reduced models only partially correct for space-clamp errors in somatic recordings of simple structures (Nadeau and Lester, 2000).

Recently, there have been advancements in the visualization and recording from dendrites (Johnston et al., 1996; Stuart et al., 1997). So far, information on dendritic channels has mainly been obtained from excised or cell-attached patch-clamp recordings (Bekkers, 2000; Bischofberger and Jonas, 1997; Hoffman et al., 1997; Korngreen and Sakmann, 2000; Magee, 1999; Magee and Johnston, 1995; Stuart and Sakmann, 1994) and from dendrosomes (Benardo et al., 1982; Kavalali et al., 1997; Takigawa and Alzheimer, 1999). However, cell-attached and outside-out recordings are laborious, and due to small currents and high variability in patch area, a large number of recordings is necessary to obtain an accurate description of dendritic channel density in such systems.

Here we present analytical, numerical, and experimental evidence, demonstrating that in general membrane conductances can be calculated from clamp-current recordings of nonregenerative conductances in a nonisopotential structure. We developed a numerical algorithm that performs this calculation and tested it on simplified potassium-channel models with systematically varied model parameters, and on a variety of potassium-channel models taken from the literature. Distortions due to the lack of space clamp were clearly seen and corrected in simulations carried out with an unbranched cylindrical cable, as well as in the soma and apical dendrite of a computer-reconstructed, layer 5 (L5) neocortical pyramidal neuron. This required i), the knowledge of morphology and passive parameters, and ii), an ionic current with hyperpolarized reversal potential. To explore the locality of the method, the cylinder was equipped with channel-density steps and gradients of various slopes were inserted into the apical dendrite of a L5 pyramidal neuron. Limitations of the correction algorithm were assessed by testing its sensitivity to incomplete knowledge of passive parameters, incorrect morphological reconstruction, and experimental noise. For voltage regions accessible to the activation voltage-clamp protocol, all channel parameters could be extracted faithfully under realistic conditions. In addition, the method was shown to be applicable to two-

*Submitted October 10, 2002, and accepted for publication December 23, 2002.*

Address reprint requests to Dr. Alon Korngreen, Faculty of Life Sciences, Bar-Ilan University, Ramat-Gan 52900, Israel. Tel.: +972-3-5318224; Fax: +972-3-5351824; E-mail: korngra@mail.biu.ac.il.



0006-3495/03/06/3508/21 $2.00

electrode voltage-clamp recordings from the apical dendrite of L5 neocortical pyramidal neurons.

## METHODS

### Simulations

All simulations were carried out using NEURON 4.1.1, 4.3.2, and 5.0.0 (Hines and Carnevale, 1997) on a Silicon Graphics Origin 2000 or on a Pentium III, 650 MHz. The integration time step used was 25 $\mu$s; changing the time step did not alter the algorithm performance provided it stayed smaller than the channel activation time constants. Potassium-channel models were taken from the literature (for a full description see Appendix): delayed rectifier $K_v$, (Mainen et al., 1995), muscarinic potassium channel $K_m$, (Mainen et al., 1995), A-type potassium channel $K_a$ (Hoffman et al., 1997), and two types of $K^+$ channels ($K_{slow}$ and $K_{fast}$), which we recently described in neocortical pyramidal neurons (Korngreen and Sakmann, 2000). Simulation data were evaluated on a Macintosh Power PC G4 using custom-written routines in IgorPro 4 (Wavemetrics; Lake Oswego, OR). The unbranched cable (cylinder) had a diameter ($d$) of 3 $\mu$m and a length ($l$) of 2000 $\mu$m (Figs. 1, 4, 5 *C* and *D*, 6, 7, and 8). When comparison with analytical calculations in an infinite cylinder was attempted during simulations, a much longer cylinder was used to approximate this situation ($d = 2$ $\mu$m and $l = 50{,}000$ $\mu$m, Figs. 2, 5 *A* and *B*, and 11). For determination of morphological parameters, a L5 neocortical pyramidal neuron of a 48-day-old Wistar rat was biocytin-filled, computer-reconstructed (except for parts of the axonal arborization), and converted to the format of NEURON as previously described (Stuart and Spruston, 1998). The passive parameters were $R_i = 250$ $\Omega$cm; $R_m = 20{,}000$ $\Omega$cm$^2$, and $C_m = 0.75$ $\mu$F cm$^{-2}$ with a passive reversal potential of $E_{leak} = -65$ mV and a potassium reversal potential of $E_k = -80$ mV, unless otherwise noted. All voltage-clamp simulations used the built-in MOD file SEClmp.mod. Dendritic two-electrode voltage-clamp configuration was simulated using the linear circuit builder in NEURON 5.0.0. Simulated voltage protocols consisted of an 8–15 s prepulse of –110 mV to relieve channels from inactivation, followed by a voltage step to the test potential. Series resistance was set to $10^{-5}$ $\Omega$ to simulate an ideal voltage clamp. The total time necessary for correcting a 100-ms voltage-clamp experiment in a full model of a layer 5 pyramidal neuron sampled at 10 kHz was 6 h on a single processor of the SGI Origin 2000 and 8 h on the Pentium III PC.

Direct contributions of the passive membrane properties were accounted for by simulating voltage-clamp experiments in morphologies that lack active conductances. Subtraction of these latter traces from those simulated in the presence of active conductances is referred to as leak subtraction. Similar results have been obtained by scaling and subtraction of currents from voltage steps to hyperpolarized potentials as performed experimentally (Augustine et al., 1985). The code of the correction algorithm can be downloaded from http://sun0.mpimf-heidelberg.mpg.de/~alon.

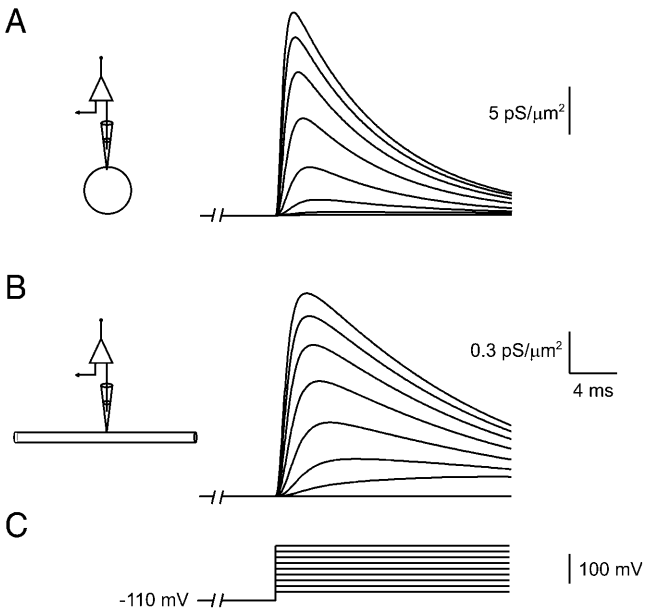


FIGURE 1 The space-clamp problem for a basic voltage-clamp protocol. A voltage protocol of 8.4 s to −110 mV (truncated to facilitate presentation), followed by a 25-ms pulse to voltages between −80 mV and +80 mV at 20 mV increments is shown in *C*. (*A*) The kinetics of the $K_{fast}$ channel as it would be recorded in an isopotential structure (short cylinder with length = 50 $\mu$m and diameter = 50 $\mu$m, *left*; density of $K_{fast}$ was 30 pS/$\mu$m$^2$). The kinetics were distorted when recorded in an unbranched cable ((*B*) long cylinder, length = 2000 $\mu$m, diameter = 3 $\mu$m; density of $K_{fast}$ was 30 pS/$\mu$m$^2$). Conductance densities were estimated by assuming that the entire membrane area contributed to the measured current (i.e., $g = I_{clamp}/((\text{total membrane area})\cdot(V_{clamp} - E))$. Note different scales.

### Slice preparation

Slices (sagittal, 300 $\mu$m thick) were prepared from the somatosensory cortex of 40–45 days old Wistar rats using previously described techniques (Stuart et al., 1993). Slices were perfused throughout the experiment with an oxygenated artificial cerebrospinal solution containing: (mM) 125 NaCl, 15 $NaCO_3$, 2.5 KCl, 1.25 $NaH_2PO_4$, 1 $MgCl_2$, 2 $CaCl_2$, 25 Glucose (pH 7.4 with 5% $CO_2$, 310 mosmol kg$^{-1}$) at room temperature (20–22°C). Pyramidal neurons from L5 in the somatosensory cortex were visually identified using infrared differential interference contrast videomicroscopy (Stuart et al., 1993).

### Solutions and drugs

The standard pipette solution contained (mM): 125 K-gluconate, 20 KCl, 10 HEPES, 4 MgATP, 10 Na-phosphocreatin, 0.5 EGTA, 0.3 GTP, and 0.2% biocytin (pH 7.2 with KOH, 312 mosmol kg$^{-1}$). The bath solution for two-electrode voltage-clamp experiments contained (mM) 125 NaCl, 15 $NaCO_3$, 2.5 KCl, 1 $MgCl_2$, 2 $CoCl_2$, 25 Glucose, 0.03 ZD2788, 0.001 tetrodotoxin (TTX pH 7.4 with 5% $CO_2$, 308 mosmol kg$^{-1}$). TTX (Tocris, Bristol, UK) was stored at −20°C as stock solutions in doubly distilled water and added directly to the bath solution. ZD2788 (Tocris) was stored at 4°C as stock solutions in doubly distilled water and added directly to the bath solution.

### Two-electrode voltage clamp

Dendritic two-electrode voltage-clamp recordings were made with an Axoclamp-2B amplifier (Axon Instruments, Foster City, CA). Two HS-2Ax0.1M headstages were used. Whole-cell recordings were performed with two patch pipettes at a distance of 30–40 $\mu$m apart. Simulations have shown that the accuracy and stability of the correction algorithm were not affected by an interelectrode distance that was smaller than 50 $\mu$m (data not shown). No series resistance compensation was used. Capacitive coupling between the electrodes was minimized by placing a grounded shield that extended almost to the bath fluid level between the electrodes. To increase clamp gain, the feedback current injected via the current injecting electrode was low pass filtered by a built-in filter of the Axoclamp-2B (phase-lag control) with a time constant of 1–5 ms. Voltage and current were filtered at 10 kHz and sampled at 50 or 20 kHz using the program ''Pulse'' (Version 8.1, Heka Electronic, Lambrecht, Germany), digitized by an ITC-16 interface (Instrutech, Greatneck, NY, USA), and stored on the hard disk of a Macintosh computer. Capacitive and leak currents were subtracted off-line by scaling of pulses taken at hyperpolarized potentials. Patch pipettes

(5–10 MΩ) were pulled from thick-walled borosilicate glass capillaries (2.0 mm outer diameter, 0.5 mm wall thickness, Hilgenberg, Malsfeld, Germany) and were coated with Sylgard before the experiment. The distance of the dendritic recording from the soma and the interelectrode distance was measured from video pictures taken by a frame grabber.

### Histology and morphology

At the end of the experiments, the slices were fixed in cold 100 mM phosphate buffer (PBS, pH = 7.4) containing 4% paraformaldehyde. After fixation, the slices were incubated for 2 h in avidin-biotinilated horseradish peroxidase (ABC Elite, Vector Laboratories, Peterborough, UK) and the stain was developed using 0.015% diaminobenzidine. The slices were mounted in Mowiol (Hoechst, Frankfurt, Germany) and stored at 4°C. The stained neurons were digitally traced using Neurolucida (MicroBrightField, Colchester, VT, USA).

### Passive membrane parameters

The passive membrane parameters ($R_m$, $R_i$, and $C_m$) were determined as previously described (Roth and Häusser, 2001; Stuart and Spruston, 1998). Briefly, before engaging the two-electrode voltage clamp, both electrodes were in bridge mode of the Axoclamp-2B. In this configuration, a 0.5 ms pulse of 0.5 nA of current was injected via one of the electrodes and the voltage deflection was monitored by both electrodes. The passive membrane properties were determined simultaneously by direct fitting of the average of 30 voltage traces measured in the same cell (Clements and Redman, 1989; Roth and Häusser, 2001; Stuart and Spruston, 1998). The fitting was carried out using NEURON by routines kindly provided by A. Roth (for details see Roth and Häusser, 2001).

## RESULTS

The voltage-clamp protocol routinely applied to measure channel activation consists of a long prepulse to a hyperpolarized voltage $V_0$, which relieves voltage-gated channels from inactivation, followed by steps to various voltages $V_1$ at which the channels activate (Fig. 1 *C*). In isopotential structures, this yields current recordings that, upon processing (i.e., leak subtraction, followed by division by the driving force and membrane area), provide changes of conductance density with time (Fig. 1 *A*). The resulting conductance densities can then be fitted to a model (Hodgkin-Huxley or other) that describes the kinetics of that channel. In nonisopotential structures this procedure results in distorted kinetics (Fig. 1 *B*) and also yields a poor prediction of channel density (note different scales in Fig. 1, *A* and *B*) since the contributing membrane area varies for different channel types in an a priori unpredictable manner. Therefore in the following, with the exception of Fig. 1, distorted currents were not converted to conductance densities, but only displayed as conductance values with different scale bars.

### The reverse problem in cable theory

Cable theory enables calculation of membrane currents in an arbitrary voltage-clamp experiment when the geometry, conductance-density distribution, and conductance kinetics are known (Rall, 1959). However, when obtaining clamp currents from voltage-clamp recordings, we are faced with the reverse problem, namely to determine the conductance kinetics, distribution, and density from the recorded currents. With a space-clamped structure, all the missing kinetic parameters can usually be extracted directly from the recorded currents, thus automatically solving the reverse problem, resulting in a full description of channel kinetics.

However, with nonisopotential structures, solution of the reverse problem is far from obvious. Our line of argument for the solution of this problem is presented in Figs. 2–4 for time-independent conductances of increasingly complex voltage dependence. In general, the reverse problem is equivalent to extracting multiple parameters (i.e., several $g_n(V_n)$ sufficient to accurately describe the conductance $g(V)$) from multiple measurements (i.e., the clamp currents $I_n$ measured in various voltage-clamp experiments). As shown below, this multiparameter problem can be split into successive one-parameter problems such that only one conductance $g_n$ at a time has to be extracted from an appropriately chosen clamp-current recording. As argued above, with the conductance $g_n$ known, the clamp current $I(g_n)$ can be calculated by cable theory. If this function is unique, it can be inverted, yielding $g_n(I_n)$, and thus solving the reverse problem. In the one-parameter case, monotonicity of the clamp current-conductance relation is sufficient for the function $I(g_n)$ to be invertible.

### Solving the reverse problem for simple conductances

A conductance with a hyperpolarized reversal potential, such as potassium, was distributed homogenously into a cylinder. A voltage clamp was applied (Fig. 2, *A* and *D*) and the steady-state situation was examined. First, a voltage-independent conductance was studied (Fig. 2, *A* and *B*). The relation between the measured clamp current $I_{clamp}$ and the underlying ohmic conductance $g$ can be determined analytically by cable theory as $I_{clamp}(g) = 2 \cdot (V - E_K)\ \sqrt{g/R_i}(\pi d^{3/2}/2)$ (diameter $d$, intracellular resistivity $R_i$, and reversal potential $E_k$ (see Koch, 1999, chapter 2, adapted from Eq. 2.17)), which is indeed monotonic for a given clamp voltage $V$ (Fig. 2 *C*).

A slightly more complex conductance was examined in Fig. 2 *E*: the conductance had a step dependence on voltage, i.e., being constant up to a voltage $V_0$ and constant again for voltages larger than $V_0$. Voltage clamping to voltages smaller than $V_0$ yields the same situation as in Fig. 2, *A–C*: The entire cable was exposed to voltages more negative than $V_0$ (Fig. 2 *D*), due to the assumption of a reversal potential at hyperpolarized voltages. Since $g(V)$ is constant throughout the entire voltage range $V < V_0$, $g$ is therefore in this experiment constant throughout the entire cable (cf. Fig. 2 *E*). Thus, $g_0 = g(V, V \leq V_0)$ can be uniquely determined from a voltage-clamp experiment with a voltage step to $V_0$ as described above for a nonvoltage-dependent conductance. In

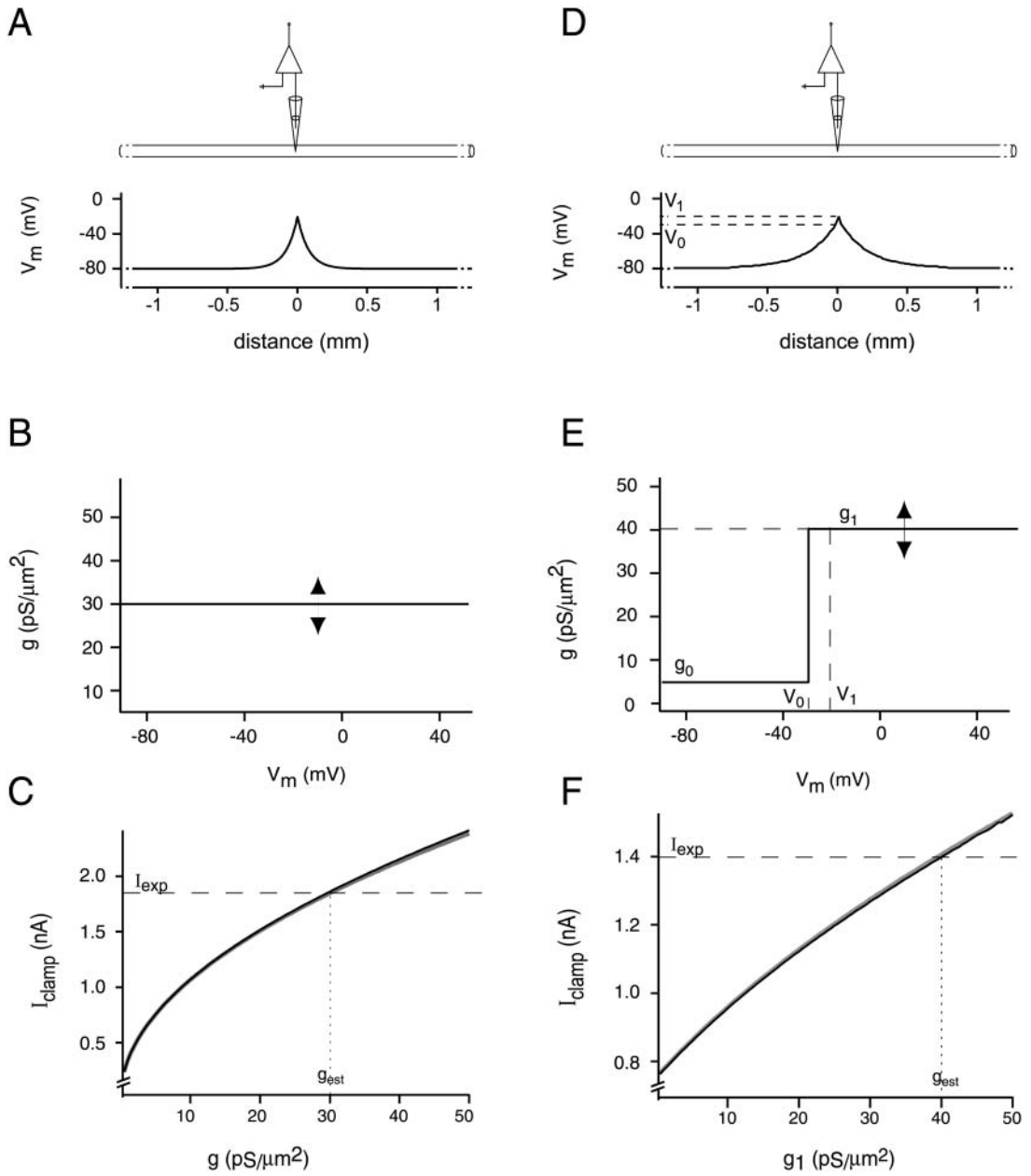


FIGURE 2 The reverse problem in steady state. (*A*) A voltage-clamp experiment was simulated in a long cable ($l = 50{,}000\ \mu$m, $d = 2\ \mu$m). The voltage attenuation in steady state is shown for a simulated voltage clamp to $-20$ mV in the middle of the cable with an ohmic membrane conductance of 30 pS/$\mu$m$^2$ (*B*). (*C*) Increasing the ohmic membrane conductance increased the required clamp current. The solid line depicts the clamp current required in simulation. For comparison, the analytical solution for an infinite cylinder with the same membrane properties is given in gray (see Appendix and Fig. 11). Comparison of the calculated clamp current with a target clamp current ($I_{exp}$, *dashed line*) resulted in a unique estimate of the underlying membrane conductance ($g_{est}$, *dotted line*). *D–F* same as *A–C* except a voltage-dependent conductance was inserted. The membrane conductance was voltage-independent, $g_0 = 5$ pS/$\mu$m$^2$ for voltages $V < -30$ mV, and $g_1 = 40$ pS/$\mu$m$^2$ for voltages $V \geq -30$ mV. (*F*) Increasing $g_1$, the membrane conductance for voltages $V \geq -30$ mV, again increased the required clamp current. The analytical solution for an infinite cylinder with the same membrane properties is given in gray (see Appendix and Fig. 11).

a second step, $g_1 = g(V, V > V_0)$ can be extracted from a voltage-clamp experiment to $V_1$: Since $g(V, V \leq V_0)$ is known from the first step, again only one parameter, $g_1$, remains to be determined. The relation between the clamp current and the conductance $g_1$ is again monotonic as shown in the Appendix (Eqs. 1, 3, and 4, Fig. 2 *F*). Therefore, also for a one-step voltage-dependent conductance as in Fig. 2 *E*, $g(V)$ can be calculated from the recorded clamp currents, solving the reverse problem.

This argument can be extended to an arbitrary conductance $g(V)$ as follows: First, consider a $g(V)$ that is a multistep function (''staircase'') with identical voltage stepwidth $\Delta V$

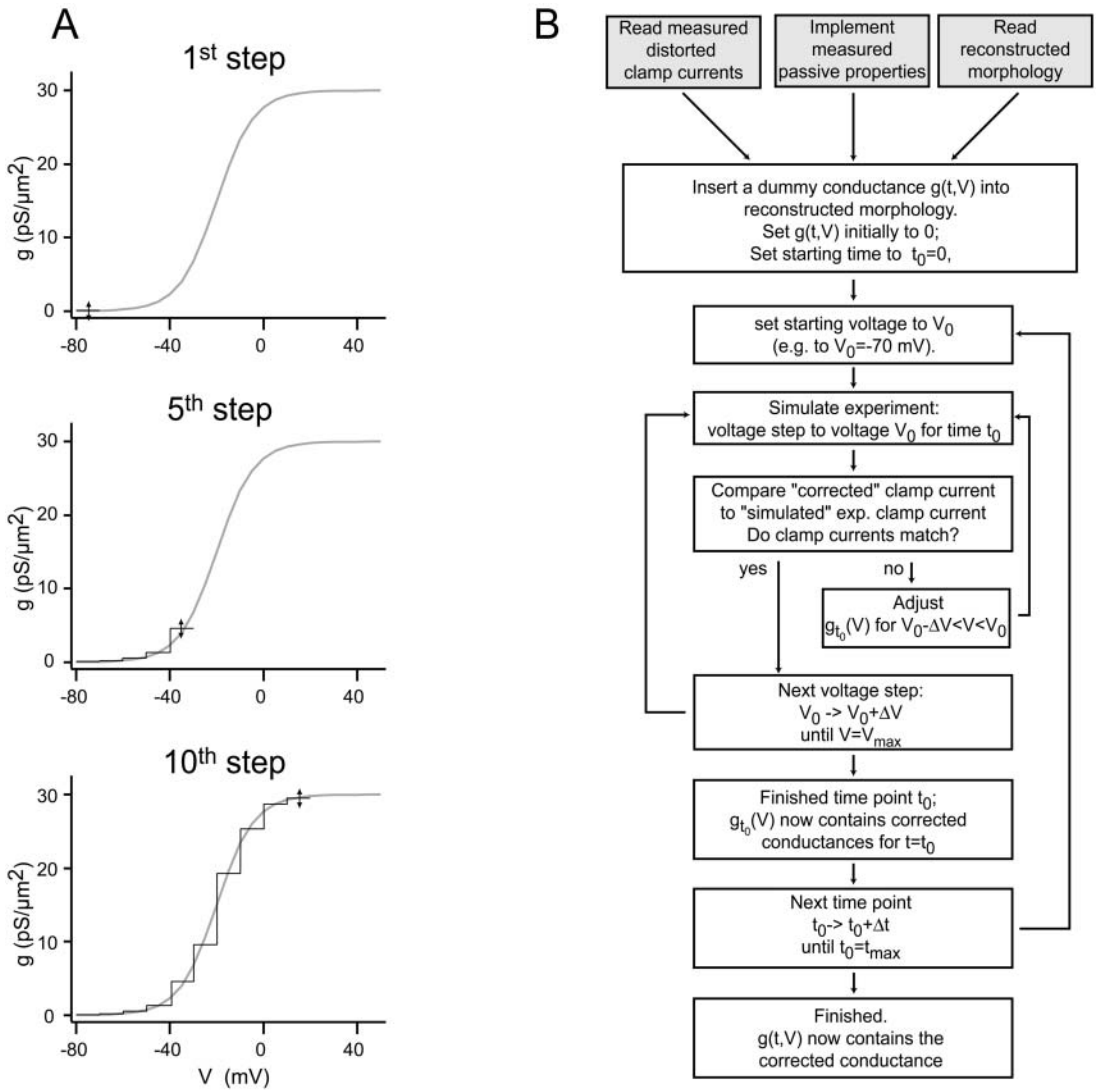


FIGURE 3 Proceeding of the correction algorithm. (*A*) Sketch of the proceeding for the correction of a Boltzmann activation curve in steady state. In the first step, the conductance between −80 mV and −70 mV was varied (*black arrow* in the *upper panel*) to fit the ''corrected clamp current'' to the ''experimentally determined current'' for a voltage-clamp experiment to −70 mV. This was repeated with successively higher voltage steps, until the estimated conductances (*black*) reflected the actual activation curve (*gray*) across the entire voltage range of interest. (*B*) Flow chart of the proceeding of the correction algorithm. The adjusting of $g(V)$ occurs either in a ''stepwise constant'' (as in *A*) or stepwise linear approximation. In the former, $g(V) = g_a$ for $V_0 - \Delta V \le V < V_0$; in the latter $g(V) = g_c + (V - V_0 + \Delta V)/\Delta V \cdot (g_a - g_c)$ for $V_0 - \Delta V \le V < V_0$. In both cases, only $g_a$ is varied to fit the ''corrected'' to the ''experimental'' clamp current. The flow chart describes the function of the entire algorithm including the correction over time. The rationale of the correction over time is described in Fig. 6. Examples and NEURON code can be downloaded from http://sun0.mpimf-heidelberg.mpg.de/~alon.

with $N$ points (e.g., *black line* in the lower panel of Fig. 3 *A*). Then we can argue the following regarding the correction of one of the conductance steps ($k$).

At the first stage of the correction ($k = 1$), assuming, that $g(V)$ is negligible for $V < V_0$, (e.g., as in Fig. 3 *A* for $V_0 < -80$ mV) a voltage-clamp experiment with a voltage step to $V_1 = V_0 + \Delta V$ will be faced with the same situation as in Fig. 2, *D–F*: Only one parameter has to be determined (that is the conductance $g_1 = g(V, V_0 < V \le V_1)$, as no voltages above $V_1$ occur and the conductance for voltages less than $V_0$ is known (i.e., assumed to be negligible). Since, as in Fig. 2, *D–F*, the relationship between clamp current and $g_1$ is monotonic (see also Appendix), $g_1$ can be determined unambiguously, thus yielding $g(V, V < V_1)$.

At the second stage of the correction ($k = 2$), performing a voltage-clamp experiment to $V_2 = V_1 + \Delta V$ results in a similar situation again: Only one parameter has to be determined as $V$ is more negative than $V_2$ in the entire structure (due to the assumption of a hyperpolarized reversal potential) and $g(V)$ is known for $V < V_1$. This missing parameter is $g_2 = g(V, V_1 < V \le V_2)$. Since the clamp current-$g_2$ relationship $I(g_2)$ is again monotonic (as

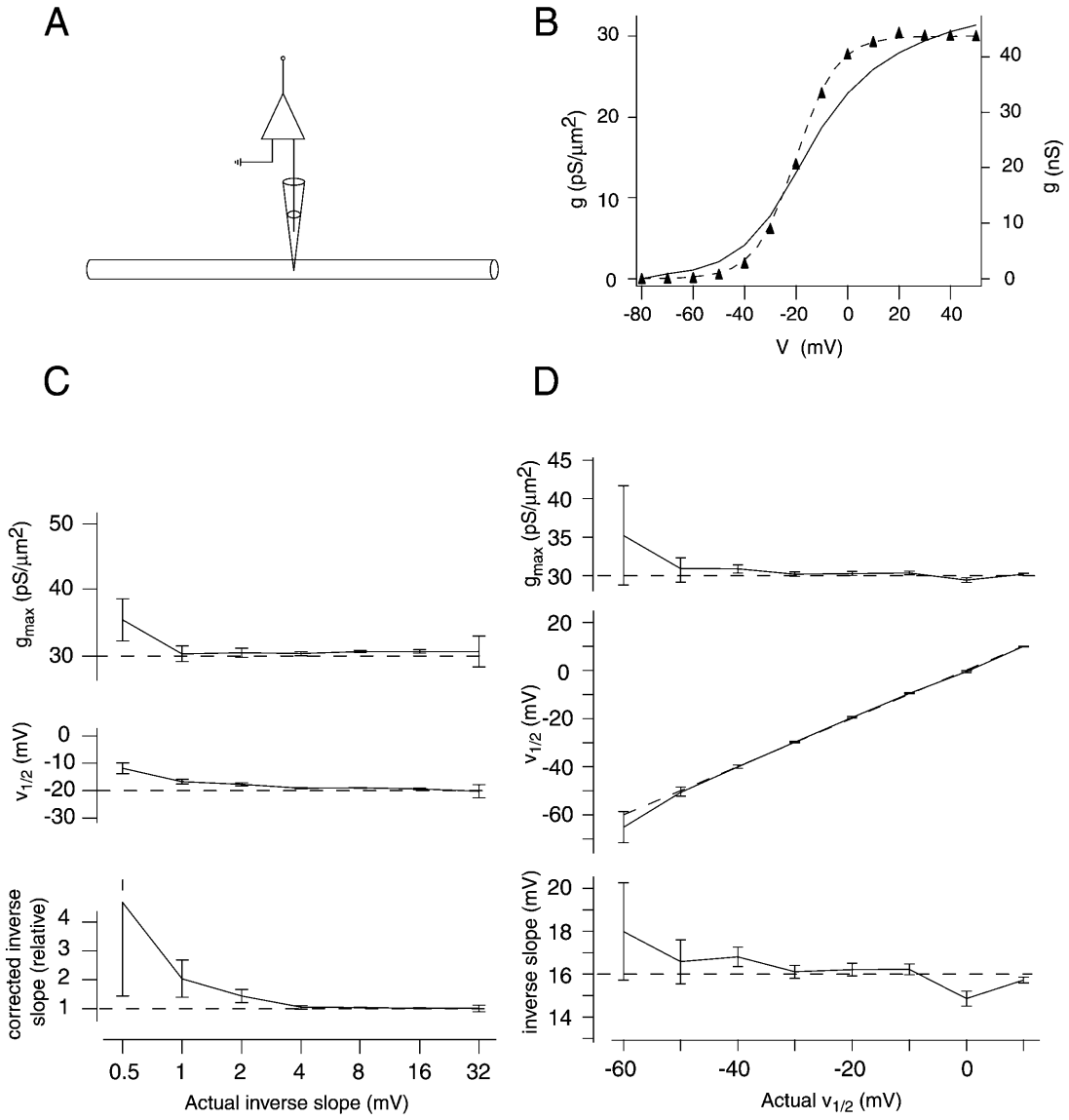


FIGURE 4 Correction of a $K^+$ channel with a Boltzmann activation curve in steady state. (*A* and *B*) A voltage-clamp experiment was simulated in a cable ($l = 2000\ \mu$m, $d = 3\ \mu$m). The clamp was inserted in the middle of the cable, and voltage steps from −110 mV to −80 mV, −70 mV . . . +60 mV were applied. The voltage-dependent membrane conductance was time-independent, and consisted of a single Boltzmann activation curve $g(V) = g_{max}/(1 + e^{-(V-V_{1/2})/k})$; $V_{1/2} = -20$ mV, $g_{max} = 30$ pS/$\mu$m$^2$, inverse slope $k = 8$ mV (*dashed line*). The solid line indicates the direct estimate of the activation curve from the distorted clamp currents (clamp currents divided by the driving force). Note the shallow slope, lack of saturation at higher voltages, and different scales (nS versus pS/$\mu$m$^2$) since normalization to the membrane area was not possible. The parameter estimates were $g_{max} = 48 \pm 1$ nS, $V_{1/2} = -14 \pm 0.8$ mV, and inverse slope $k = 15.8 \pm 0.8$ mV. The corrected conductance densities are depicted as triangles ($g_{max} = 30.3 \pm 0.1$ pS/$\mu$m$^2$, $V_{1/2} = -19.1 \pm 0.1$ mV, inverse slope $= 8.2 \pm 0.1$ mV). The voltage-clamp experiment was simulated for different slopes (*C*) and different $V_{1/2}$ (*D*) of the Boltzmann activation curve. The three conductance parameters that fully describe the conductance were calculated from a Boltzmann fit to the corrected conductance-voltage relation (*triangles* in *B*). Error bars indicate the goodness of the Boltzmann fit depicted as standard deviation in fit parameters estimated from the residuals. The actual parameters of the underlying conductances are shown as dashed lines.

in Fig. 2, cf. Appendix), $g_2$ can be determined from the clamp current, resulting in the knowledge of $g(V)$ for all voltages up to $V_2$: $g = 0$ for $V \le V_0$, $g = g_1$ for $V_0 < V \le V_1$; $g = g_2$ for $V_1 < V \le V_2$. At this step, $g$ is still unknown for voltages above $V_2$.

At the rest of the correction stages ($2 < k < N$), continuing this procedure in steps of $\Delta V$ results in a stepwise calculation of $g(V)$ for all voltages of interest. The conductance $g(V, V_{n-1} < V \le V_n)$ can be calculated from a voltage step to a voltage $V_n = V_{n-1} + \Delta V$, relying on the knowledge of $g(V, V \le V_{n-1})$ from previous calculation steps (see Fig. 3). Essentially every smooth function $g(V)$ can be approximated by a multistep "staircase" function with sufficiently small stepwidth

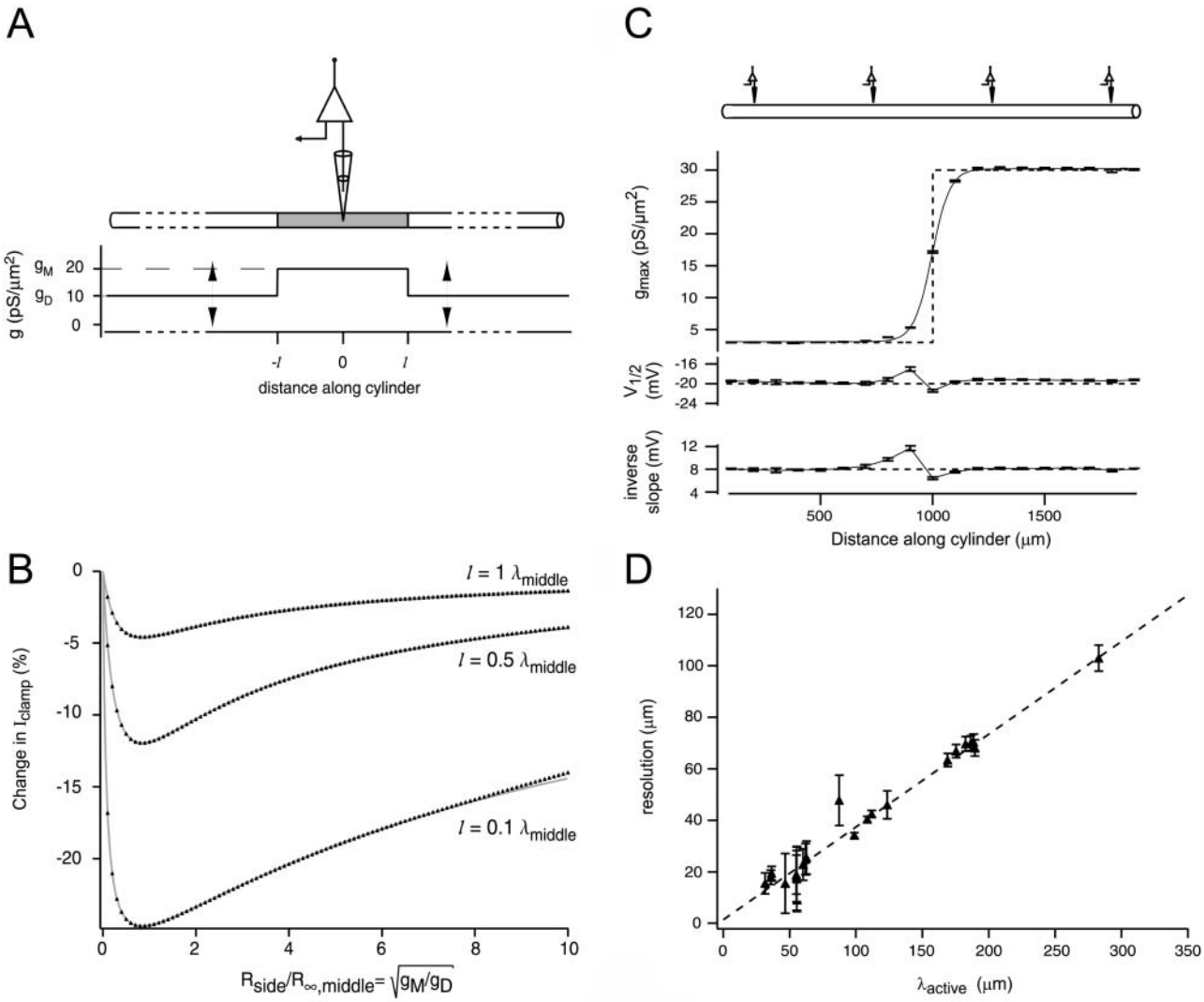


FIGURE 5 Spatial resolution. (*A*) A voltage-clamp experiment was simulated in a long cable as in Fig. 2. Distances were measured from the position of the clamp. The cable was equipped with an ohmic conductance of $g_D = 10$ pS/$\mu$m$^2$ for distances greater than $l$ and $g_M = 20$ pS/$\mu$m$^2$ around the clamp electrode. (*B*) $g_D$ was decreased by 50%, and the ensuing change in the steady-state clamp current was calculated both analytically (*gray line*) and by simulation (*black dots*) for various $g_D$ (see Appendix). This was repeated for three different distances $l$. $R_{side}$ is the input resistance of the white cylinders, and $R_{\infty,middle}$ the input resistance of a semi-infinite cylinder with the properties of the middle, gray cylinder. Therefore, $R_{side}/R_{\infty,middle} = \sqrt{g_M/g_D}$; $\lambda_{middle}$ indicates the space constant of the middle cylinder $\lambda_{middle} = \sqrt{1/(R_a \cdot g_M) \cdot d/4}$. (*C*) A voltage-clamp experiment was simulated in a cable equipped with a Boltzmann-like conductance as in Fig. 4. The conductance density, $g_{max}(x)$, was $g_0$ for $x < 1000$ $\mu$m and $g_1$ for $x \geq 1000$ $\mu$m. For each position, the simulated clamp currents were corrected assuming a homogenous conductance distribution. The corrected $g(V)$ obtained was analyzed as in Fig. 4. Therefore, for each electrode position, three parameters could be obtained, that attempt to fully describe the underlying voltage-dependent conductance. Error bars indicate the goodness of the Boltzmann fit to the corrected conductance densities depicted as standard deviation in fit parameters. The estimate of the corrected conductance density (*dots*) deviates from the actual step function (*dashed line*) and was fitted with a sigmoid (*thin line*). (*D*) Voltage-clamp experiment and correction were repeated for various combinations of $g_0$, $g_1$, $R_a$, and $R_m$. The spatial resolution of the correction was calculated as the inverse slope parameter of the sigmoid. For every parameter combination, the space constant $\lambda_{active}$ was determined as $\lambda_{active} = \sqrt{1/(R_a \cdot g_{Membrane}) \cdot d/4}$, with the membrane conductance $g_{Membrane} = (1/R_m)/2 + (g_0 + g_1)$. Error bars indicate the goodness of the sigmoidal fit depicted as standard deviation in fit parameters.

$\Delta V$. Thus, in approximation, the reverse problem in a cylinder can be solved for any voltage-dependent conductance (with little activation at hyperpolarized potentials and a hyperpolarized reversal potential) by applying successive voltage-clamp experiments and using the data obtained from previous experiments to process current recordings for higher voltages.

## The correction algorithm

To implement the approximation technique described above, we relied on i), accurate knowledge of passive properties and morphology (discussed in detail below); ii), the ionic current being nonregenerative (i.e., the reversal potential being below the region of activation for this channel—for

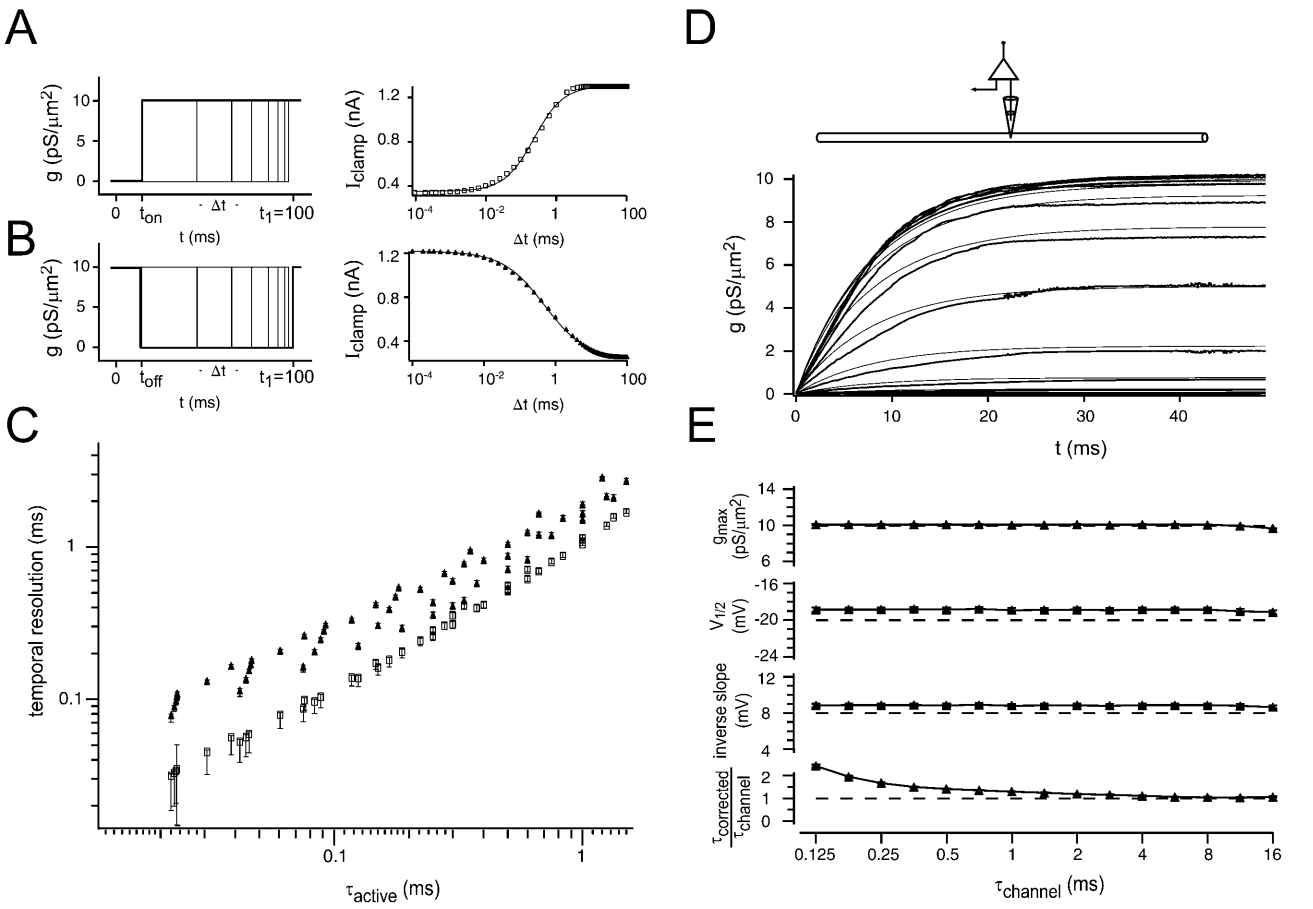


FIGURE 6 Temporal resolution. (*A*) Step conductance. A voltage-clamp experiment was simulated in a cable as in Fig. 4. The voltage clamp was inserted in the middle of the cable, and consisted of a voltage step from −80 mV to 0 mV. Time was measured from the beginning of the voltage step. The cable was equipped with an ohmic conductance; $g(t) = 0$ for $t < t_{on}$, and $g(t) = 10\ \mathrm{pS}/\mu\mathrm{m}^2$ for $t > t_{on}$ (*left panel*). The clamp current was calculated and plotted against $\Delta t = 100\ \mathrm{ms} - t_{on}$ (*squares*). The temporal resolution was defined as the half maximum of a sigmoid fit (*thin line*, *right panel*) to the clamp current-*log*$\Delta t$ relation. (*B*) Gap conductance: Same conditions as in *A*, except the cable was equipped with an ohmic conductance of $g(t) = 10\ \mathrm{pS}/\mu\mathrm{m}^2$ for $t < t_{off}$, $g(t) = 0$ for $t_{off} \le t < 100$ ms, and $g(t) = 10\ \mathrm{pS}/\mu\mathrm{m}^2$ again for $t > t_{off}$ (*left panel*, thus resulting in a time window (''gap'') when the conductance is not active). The clamp current was calculated and plotted against $\Delta t = 100\ \mathrm{ms} - t_{off}$ (*triangles*). (*C*) The temporal resolution was determined for situations as depicted in *A* (*squares*) and *B* (*triangles*) for various peak conductances, $R_m$ and $C_m$. The $\tau_{active}$ was calculated as: $\tau_{active} = C_m/g_{Membrane}$, with $g_{Membrane} = (g_{Peak}/2) + (1/R_m)$. (*D*) A voltage-clamp experiment was simulated as in Fig. 4. Conductances are shown for every second voltage step only. The voltage-dependent membrane conductance was time-dependent: $dg(V,t)/dt = -(g(V,t) - g_\infty(V))/\tau_{channel}(V)$, with $g_\infty(V) = g_{max}/(1 + e^{-(V-V_{1/2})/k})$, $V_{1/2} = -20$ mV, $g_{max} = 10\ \mathrm{pS}/\mu\mathrm{m}^2$, inverse slope $k = 8$ mV, and $\tau_{channel}(V) = 8$ ms (shown in *gray*), thus the conductance could be fully characterized by four parameters. Corrected conductances were determined independently for each time point without a priori knowledge about the kinetic structure of the underlying conductance. (*E*) The simulation and correction described in *D* was repeated for a conductance with systematically varied activation time constants ($\tau_{channel}$). The 50-ms time points of the resulting corrected conductances were fitted as in Fig. 4 to determine $g_{max}$, $V_{1/2}$, and inverse slope. The corrected $\tau$, which was obtained by fitting a single-exponential rise to the −10 mV conductance trace, is depicted normalized to the actual underlying $\tau_{channel}$. The actual conductance parameters are shown for comparison (*dashed lines*). Error bars indicate the goodness of the sigmoidal and exponential fit depicted as standard deviation in fit parameters.

simplicity, a potassium current with a hyperpolarized reversal potential was assumed); and iii), the conductance being negligible at resting membrane conditions, so that $g(V, V < -80\ \mathrm{mV}) = 0$ could be assumed as a starting condition. In the first step of the correction algorithm, the conductance between −80 mV and −70 mV (that was assumed to be constant throughout this voltage range) was determined from the clamp current $I_1$ obtained from a voltage-clamp protocol stepping from −110 mV to −70 mV (see Fig. 1 *C*). This was achieved by simulating the voltage-clamp experiment in the given morphology with a time-independent potassium conductance that was different from 0 (but constant $g_1$) only for voltages above −80 mV. The magnitude $g_1$ of the potassium conductance was varied systematically to minimize the squared difference $(I_{clamp,simulated} - I_{exp,1})^2$ (using the golden section algorithm (Press et al., 1992)).

In the next step, the conductance was now known between −80 mV and −70 mV from the first correction step and assumed constant again but yet unknown for the next voltage region from −70 mV to −60 mV, in analogy to Fig. 2, *D–F*. The conductance for this more depolarized voltage region could again be obtained from the voltage-clamp data, this time

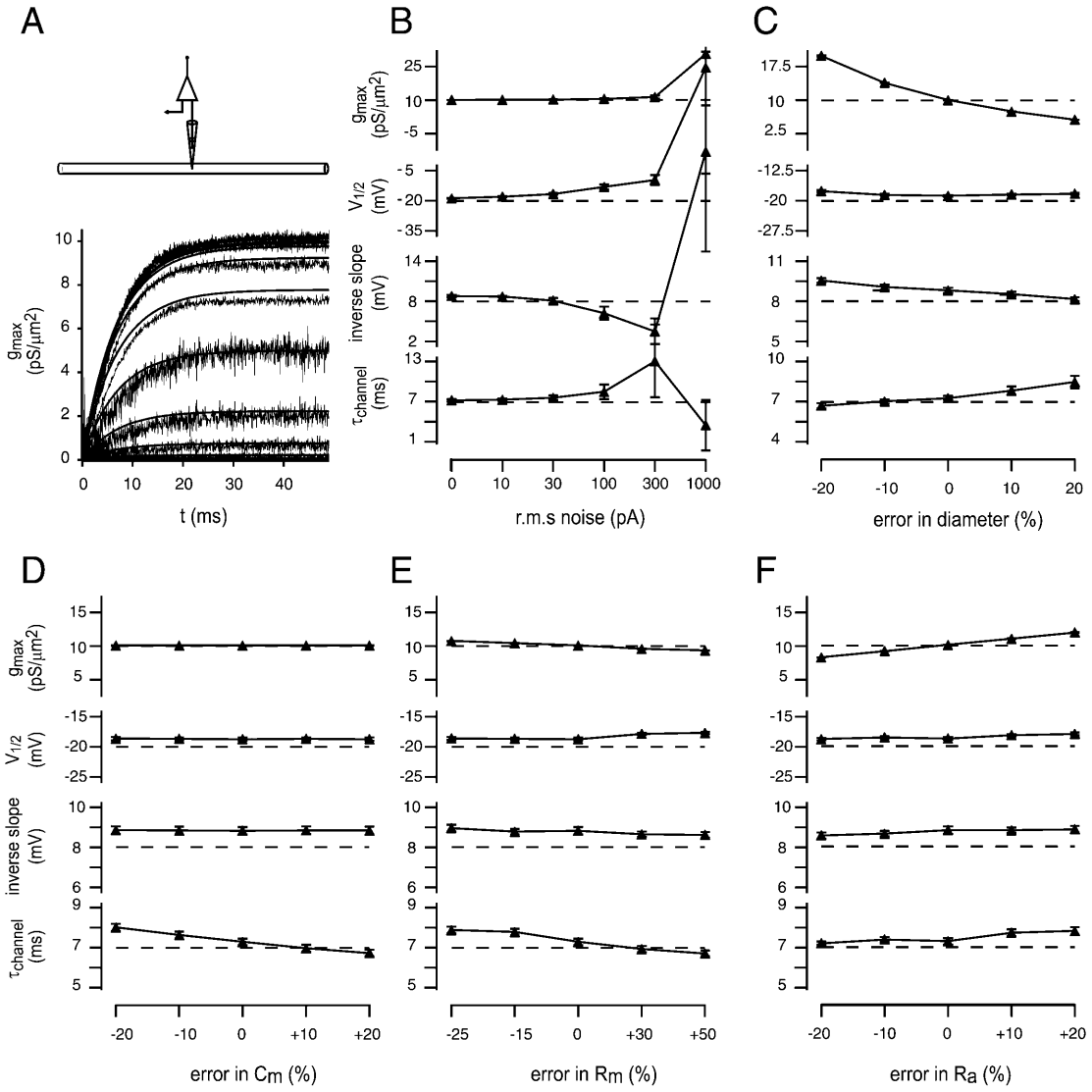


FIGURE 7 Effects of noise and incomplete knowledge of passive parameters on performance of the correction algorithm. (*A*) A cylinder was prepared as in Fig. 6 *D*; conductance parameters were $V_{1/2} = -20$ mV, $g_{max} = 10$ pS/$\mu$m$^2$, inverse slope = 8 mV, and $\tau_{channel} = 7$ ms. A voltage-clamp experiment was simulated, and random Gaussian noise added (10 pA rms) to the simulated currents. The corrected conductance estimate was plotted (*thin lines*) and compared to the true conductance (*thick lines*). (*B*) Noise of increasing magnitude was added to the recordings. The resulting corrected conductances were analyzed as described for Fig. 6 *D* and compared to the actual conductance parameters (*dashed lines*). (*C–F*) During the correction, passive parameters were changed in comparison to the simulated experiment, as indicated by the ''% error'', to emulate inaccurate knowledge of the underlying parameters. Conductance parameters were calculated from the corrected conductances as described for Fig. 6 *D* and compared to the actual conductance parameters (*dashed line*). Note the different scales for the channel parameter errors in *C* compared to *D–F*.

using the recorded clamp current $I_2$ for a voltage step from $-110$ mV to $-60$ mV. Again, simulations of the voltage-clamp experiment were performed in the given morphology with the potassium conductance $g = 0$ (for $V \leq -80$ mV); $g = g_1$ (for $-80$ mV $< V \leq -70$ mV), and $g =$ variable (for $-70$ mV $< V \leq -60$ mV; higher voltages did not occur due to the assumption of a hyperpolarized reversal potential). To obtain $g_2 = g(V, -70\,\text{mV} < V \leq -60\,\text{mV})$, it was varied to minimize the difference $(I_{\text{clamp,simulated}} - I_{\text{exp,2}})^2$.

This process was continued in 10 mV steps until the entire activation curve $g(V)$ of the conductance was retrieved by this approximation technique (Fig. 3 *A*). In the following, the accuracy was increased by replacing the stepwise constant approximation with a stepwise linear approximation of the conductance (see also legend to Fig. 3 *B* and Appendix). As the voltage profile narrowed with increasing voltage, the step size was increased to 20 mV for $(V - E_k) > 80$ mV, i.e., $V > 0$ mV.

In general, rather than correcting distorted clamp currents, then converting the corrected current to a conductance and finally to a conductance density, the algorithm is used to directly estimate the conductance density to fit the resulting clamp currents to the ''experimentally recorded'' ones.

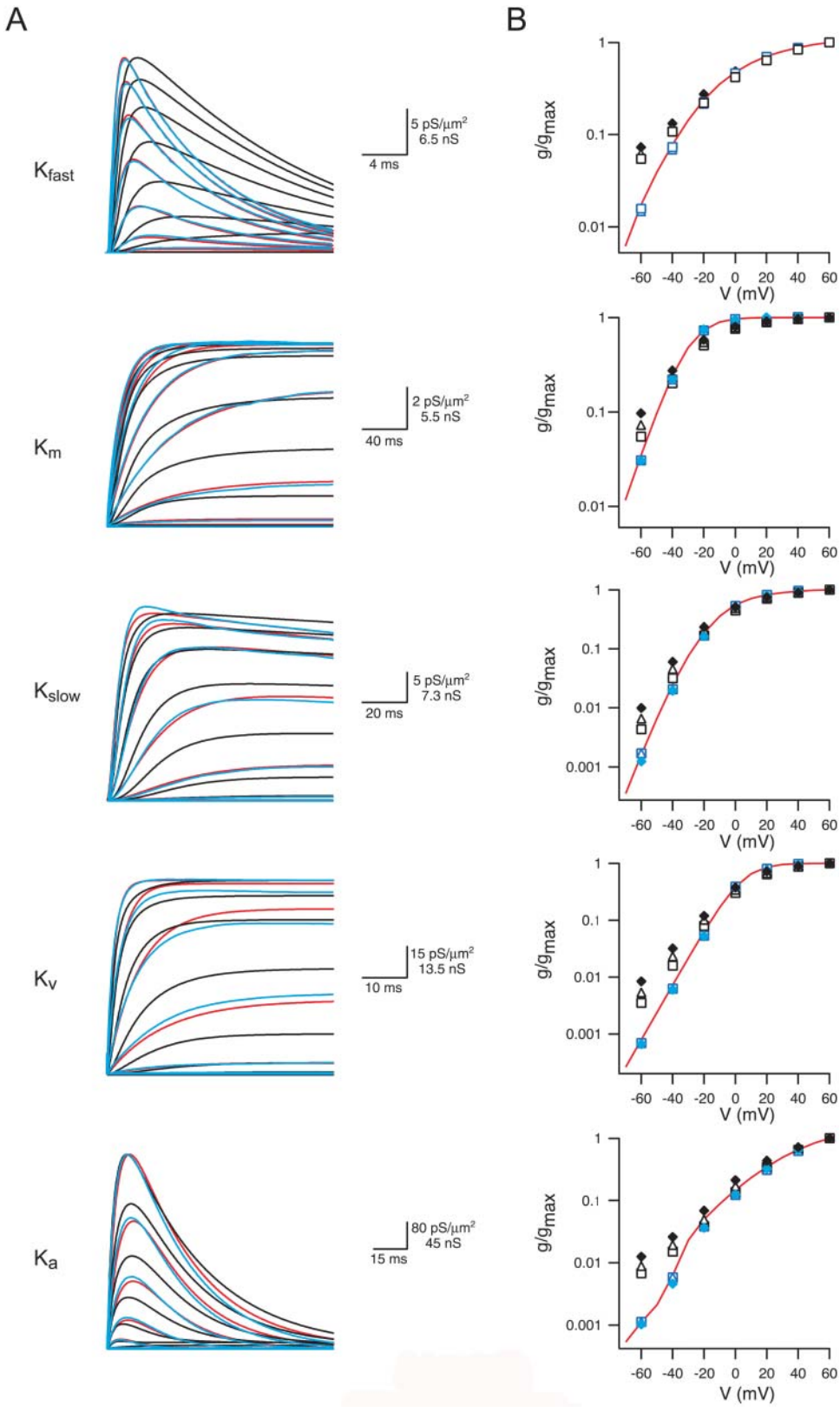


FIGURE 8 Space-clamp distortions and corrections for realistic potassium conductances in a cable. The uncorrected currents were simulated as in Fig. 4, with 30 pS/$\mu$m$^2$ of $K_{fast}$, 10 pS/$\mu$m$^2$ of $K_m$, 30 pS/$\mu$m$^2$ of $K_{slow}$, 100 pS/$\mu$m$^2$ of $K_v$, and 100 pS/$\mu$m$^2$ of $K_a$. The prepulse (for 8.4 s to –110 mV) was truncated to facilitate presentation. The current was corrected for the passive leak, and converted to a conductance by dividing by the driving force (*A*, *black lines*). The conductance-density estimates obtained with the correction algorithm are displayed as blue lines. For comparison, the true kinetics are shown as red lines in all panels. Scale bars apply to the (uncorrected) conductance in the left panel (conductance in nS), and to the true kinetics and corrected traces (conductance density in pS/$\mu$m$^2$). (*B*) Cables as in *A* were prepared with different conductance densities ($K_{fast}$: 3, 10, and 30 pS/$\mu$m$^2$; $K_m$: 1, 3, and 10 pS/$\mu$m$^2$; $K_{slow}$: 3, 10, and 30 pS/$\mu$m$^2$; $K_v$: 10, 30, and 100 pS/$\mu$m$^2$; and $K_a$: 10, 30, and 100 pS/$\mu$m$^2$). Peak conductances were calculated from the corrected kinetics, normalized to the value at +60 mV, and shown as blue markers in *B* for the three conductance densities (low (*open squares*), medium (*open triangles*), and high (*solid diamonds*)). The uncorrected conductances are shown in black symbols similar to those used to describe the corrected conductance. The red lines were calculated directly from the original kinetics ($K_{fast}$: 5 pS/$\mu$m$^2$; $K_m$: 10 pS/$\mu$m$^2$; $K_{slow}$: 5 pS/$\mu$m$^2$; $K_v$: 100 pS/$\mu$m$^2$; and $K_a$: 100 pS/$\mu$m$^2$). The pseudo-steady-state approach was modified for these simulations by replacing the constant, time-independent conductance model with a mono-exponential one. The necessary time constants ($\tau$) were roughly estimated as the rise time of the distorted clamp-current recordings (half the time in which 86% of the peak current was reached). Changing $\tau$ up to 10-fold did not significantly alter the correction result.

## Testing the algorithm

To test the algorithm, we used known conductances to obtain simulated voltage-clamp currents, distorted by a lack of space clamp. Here, the term ''simulated currents/conductances'' refers to these currents, and the term ''corrected currents/conductances'' describes currents/conductances generated by the correction algorithm. It has to be emphasized that the simulated currents were analyzed by the correction algorithm without any prior knowledge of the kinetics or distribution of the conductance that had been used to generate them.

First, a simple time-independent potassium conductance was implemented in an unbranched cable (Fig. 4 *A*). Its Boltzmann activation curve is depicted in Fig. 4 *B* (*dashed line*; $g_{max} = 30$ pS/$\mu$m$^2$, $V_{1/2} = -20$ mV, inverse slope = 8 mV). Direct estimation of the activation parameters from the distorted clamp-current recording (*solid line* in Fig. 4 *B*) yielded a shallow slope and no saturation at high voltages. However, the correction algorithm accurately retrieved the activation parameters: $g_{max} = 30.3 \pm 0.1$ pS/$\mu$m$^2$, $V_{1/2} = -19.1 \pm 0.1$ mV, inverse slope = $8.2 \pm 0.1$ mV. The range of parameters that can be accurately retrieved was assessed systematically by varying the slope and $V_{1/2}$ of the activation curve (Fig. 4, *C* and *D*, respectively). Steep activation curves yielded increasingly worse fits for inverse slopes smaller than 2 mV (i.e., 25–75% activation within 4 mV). For shallow activation curves with inverse slopes >32 mV, a decrease of the accuracy of the fit was observed as a result of significant activation at the starting potential ($V$ = –80 mV). When $V_{1/2}$ was varied (Fig. 4 *D*), accurate values for all Boltzmann parameters were retrieved for $V_{1/2} > -40$ mV. For smaller values of $V_{1/2}$, once again significant activation at –80 mV resulted in deviations from the original Boltzmann activation curve. Similar results were obtained with a nonmonotonic conductance-voltage relation $g(V) = 10\ \text{ps}/\mu\text{m}^2/(1 + \exp((V + 10\ \text{mV})/20\ \text{mV})^2)$ (data not shown).

These findings indicate that our correction algorithm is capable of extracting steady-state activation parameters in a non-space-clamped situation for all but extremely steeply activating channels or those with a substantial activation at rest. Thus, the algorithm can in principle solve the reverse problem.

## Spatial resolution of the algorithm

In realistic situations, the membrane properties are neither known completely nor necessarily homogenous. Thus, we investigated whether i), distal regions of unknown structure affect the precision of the algorithm, and whether ii), the obtained activation curve reflects local membrane properties or rather some average across parts of the structure.

These concerns were assessed by first studying the influence of changes in distal membrane properties on clamp-current recordings (see Fig. 5, *A* and *B*, and Appendix). A cylinder was divided into a middle region and two distal ones (Fig. 5 *A*). For simplicity, these cylindrical regions were modeled with constant membrane conductances $g_M$ and $g_D$, respectively. Then, $g_D$ was varied and the relative change in $I_{clamp}$ was noted for different $g_M/g_D$ (or $R_{side}/R_{\infty,middle}$, cf. Appendix) ratios. Even when the distal region was as close as $(1/2)\lambda_{middle}(\lambda_{middle} = \sqrt{(1/R_i \cdot g_M) \cdot (d/4)})$, 50% changes of the distal membrane conductance $g_D$ did not alter $I_{clamp}$ by more than 12% (Fig. 5 *B*, *middle trace*). The alteration of $I_{clamp}$ was most prominent for situations where $g_D$ approximately equaled $g_M$ (Fig. 5 *B*).

In addition, a spatial conductance step was implemented in a cylinder. The simulated clamp currents at various positions (Fig. 5 *C*) were corrected without any a priori assumptions about the channel distribution. Since channel distributions are in general not known in an experimental situation, a homogenous channel distribution was assumed for correction of the individual recordings at different positions. The corrected conductance parameters for a conductance step from 3 to 30 pS/$\mu$m$^2$ at various positions are depicted in Fig. 5 *C*: Both $V_{1/2}$ and the inverse slope of the activation curve were retrieved accurately throughout the cylinder. Deviations from the actual values (*dashes*) were small and occurred primarily close to the conductance step. The conductance density was retrieved as a sigmoid, whose inverse slope indicated the spatial resolution of the correction algorithm. Repetition of this simulation and correction procedure for various conductance densities and passive parameters showed the dependence of the resolution on the ''active space constant'', $\lambda_{active}$. This term refers to the apparent space constant when voltage-gated channels are open, $\lambda_{active} = \sqrt{g_{pas}/g_{act}} \cdot \lambda_{pas}$. For $R_m = 30{,}000\ \Omega\text{cm}^2$ ($g_{pas} = 0.33$ pS/$\mu$m$^2$) and $g_{act} = 30$ pS/$\mu$m$^2$, $\lambda_{active} \approx \sqrt{0.01} \cdot \lambda_{pas}$, which is only 10% of the passive space constant. Thus, information obtained was averaged over a small region that extended only on the order of $\lambda_{active}$ around the recording electrode (Fig. 5 *D*).

## Temporal resolution of the algorithm

The applicability of the algorithm to non-steady-state situations was tested by studying the sensitivity of clamp-current recordings to temporal changes in channel activation, and in addition by correcting clamp-current recordings from potassium channels with various activation times. For the non-steady-state case, we have to assume a kinetic model for the time course of $g(V,t)$, this model being as simple as possible. Therefore, clamp currents recorded during activation of voltage-gated channels were corrected independently for every time point $t_1$: For each $t_1$, we assumed a simple kinetic ''model'' $g = const$ for all times less than $t_1$ and approximated the voltage-dependent conductance $g(V)$ to fit the corrected clamp current at time $t_1$ to the simulated current, thus obtaining the activation curve at time $t_1$: $g(V,t_1)$.

This was repeated independently for each time point to yield the complete activation kinetics $g(V,t)$ as outlined in Fig. 3.

To assess the errors made by this ''pseudo-steady-state'' approach, the dependence of the clamp current on the recent history of the membrane conductance was examined. A voltage clamp with a voltage step from −80 mV to 0 mV at $t = 0$ was performed, and the clamp current was measured at $t_1 = 100$ ms. Then a constant membrane conductance was implemented in the cylinder and switched on at varying times $t_{on}$, $0 < t_{on} < t_1$ (Fig. 6 *A*). This conductance made the clamp current change as a function of $\Delta t = t_1 - t_{on}$. The half maximum of a log-sigmoid fit to $I_{clamp}(\Delta t)$ yielded a measure of the temporal resolution (''memory'') of the clamp-current recording. The same procedure was applied to a conductance that was initially on, switched off at varying times $t_{off}$, and on again at $t_1 = 100$ ms (Fig. 6 *B*), and to a conductance that increased linearly from 0 at time $t_{on}$ to a maximum value at $t_1 = 100$ ms (data not shown). The dependence of the temporal resolution of the system on the apparent membrane time constant upon activation of all conductances (active membrane time constant: $\tau_{active}$, cf. legend to Fig. 6) is shown in Fig. 6 *C*.

Active time constants are usually small ($\tau_{active} \approx 300\ \mu s$ for a conductance with a density of 30 pS/$\mu m^2$), which encouraged us to take the approach described above, i.e., not to assume a special kinetic model for the underlying conductances, but rather to fit every time point independently with a time-independent conductance. The fitted conductance is expected to reflect the time course of the actual underlying conductance with an accuracy of about $\tau_{active}$.

The validity of this ''pseudo-steady-state'' approach was further assessed by implementing a simplified potassium-channel model in a cable (Fig. 6 *D*). This channel model consisted of one activation particle with a voltage-independent activation time ($\tau_{channel} = 8$ ms) and a first-order steady-state activation model as in Fig. 4 ($g_{max} = 10$ pS/$\mu m^2$, $V_{1/2} = -20$ mV, inverse slope = 8 mV). Channel kinetics directly estimated from the simulated distorted clamp currents deviated from the actual values ($V_{1/2} = -12.8 \pm 0.8$ mV, inverse slope = 15.6 ± 0.7 mV, $\tau_{channel} = 10.4 \pm 0.1$ ms; $\tau_{channel}$ was determined for the voltage step to −10 mV). In contrast, by using the correction algorithm, the channel parameters could be retrieved accurately ($g_{max} = 10.10 \pm 0.04$ pS/$\mu m^2$, $V_{1/2} = -18.7 \pm 0.2$ mV; inverse slope = 8.9 ± 0.2 mV and $\tau_{channel} = 8.8 \pm 0.4$ ms). Variation of $\tau_{channel}$ indicated that, for all activation time constants, the steady-state parameters were determined correctly (Fig. 6 *E*). However, estimation of the channel activation time was less precise for fast channels ($\tau_{channel} < 300\ \mu s$), which confirmed the prediction based on Fig. 6 *C*. Higher or lower channel densities (from 1 to 1000 pS/$\mu m^2$) or membrane resistances (from 2000 to 128,000 $\Omega cm^2$) did not influence algorithm performance (not shown).

## Sensitivity and numerical stability

The algorithm, due to its structure, cannot be tested analytically for numerical stability. Therefore, stability was tested by adding various white noise levels to a simulated current recording from a cylinder with a simple underlying conductance (Fig. 7 *A*; $g_{max} = 10$ pS/$\mu m^2$, $V_{1/2} = -20$ mV, inverse slope = 8 mV, $\tau_{channel} = 7$ ms). The corrected conductance density for a noise level with root mean square (rms) of 10 pA (~1% of steady-state current at 0 mV) is depicted in Fig. 7 *A*. The original kinetics were easily retrieved. The activation curve was markedly distorted only for noise levels above 100 pA rms. (Fig. 7 *B*). Thus, for experimentally observed noise levels numerical stability of the algorithm can be obtained.

The sensitivity of the correction algorithm to morphological and electrical parameters was also examined. Recordings from a cylinder, equipped with the same conductance as in Fig. 7 *A*, were made with the same passive parameters as described above. However, for the correction algorithm, passive parameters were modified, thus simulating an incorrect estimate of the true passive parameters. Global increases or decreases in the diameter of the cylinder were used to simulate incorrect morphological reconstruction. Changes in the corrected conductance parameters occurred mainly with incomplete knowledge of the morphology (Fig. 7 *C*, compare to 7, *D–F*). Overall, neither noise nor variations in passive parameters or morphology to an extent expected from experimental accuracy resulted in significant deviations of the correction results from the actual underlying channel parameters.

## Full channel models

The correction algorithm was tested on more complex channel kinetics by implementing several published models of potassium channels in a 2-mm long cable. Simulations of voltage-clamp experiments produced clamp currents with distortions due to lack of space clamp (*black* in Fig. 8 *A*). As expected, apparent activation and inactivation time constants increased and the voltage dependence of the steady-state conductance flattened. The correction algorithm yielded estimates for the conductance kinetics (*blue trace* in Fig. 8 *A*) that accurately reflected the underlying channel properties (*red trace* in Fig. 8 *A*). The kinetics of fast inactivating channels ($K_{fast}$ and $K_a$) and channels with a steep conductance-voltage relation ($K_v$) were not corrected as properly as slower channels ($K_m$ and $K_{slow}$). This deviation corresponded to the predictions depicted in Figs. 4 and 6. The contributing membrane areas varied significantly, thus no a priori prediction could be made for the conductance densities. Therefore, the distorted currents are displayed as conductances rather than conductance densities and with different scales to facilitate comparison. The results of applying the algorithm to several conductance densities of each of the five realistic

conductances ($K_{fast}$: 3, 10, and 30 pS/$\mu$m$^2$; $K_m$: 1, 3, and 10 pS/$\mu$m$^2$; $K_{slow}$: 3, 10, and 30 pS/$\mu$m$^2$; $K_v$: 10, 30, and 100 pS/$\mu$m$^2$; and $K_a$: 10, 30, and 100 pS/$\mu$m$^2$) are shown in Fig. 8 *B*. The maximal conductance obtained at each voltage was normalized to the conductance at the maximal voltage ($V = 60$ mV). The results obtained by applying the algorithm to these realistic channels demonstrated that correcting every time point independently is sufficient to accurately obtain the kinetics of a wide range of potassium channels.

## Correcting in neuronal morphologies

The major goal in designing the correction algorithm was to devise a method that could overcome space-clamp problems in elongated and branched structures, such as large cortical neurons. Therefore, the algorithm was tested on a fully reconstructed L5 neocortical pyramidal neuron (Fig. 9 *A*), into which was inserted the fast inactivating potassium channel $K_{fast}$ (Korngreen and Sakmann, 2000). This type of neuron was selected for the simulations because it provided a worst case of problems that arise from improper space clamp. As expected, in somatic recordings the uncorrected conductance calculated from currents that were obtained from a simulated somatic voltage clamp did not properly reflect the underlying kinetics (Fig. 9 *A*, *bottom panel*, *black* versus *red traces*). In this morphology, as with the cylinder, application of the correction algorithm considerably reduced the error (Fig. 9 *A*, *bottom panel*, *blue traces*). The same was true for simulated currents from the apical dendrite (Fig. 9 *A*, *upper panels*). Note that the uncorrected dendritic currents obtained at the indicated positions not only display distorted kinetics, but also incorrect values of the relative channel densities (Fig. 9 *A*, *black traces*).

In both hippocampal (Hoffman et al., 1997) and neocortical (Korngreen and Sakmann, 2000) pyramidal neurons, potassium-channel densities change along the apical dendrite. Therefore, we tested whether the correction algorithm could retrieve correct local conductance densities without a priori knowledge of a conductance density gradient. The same reconstructed pyramidal neuron was used with a $K_{fast}$ conductance density that was constant across soma, axon, and basal dendrites, but increased linearly along the apical dendrite. Again, uncorrected conductances from several recording sites as in Fig. 9 *A* displayed distorted channel kinetics (not shown). For the correction algorithm, a homogenous density of potassium channels was assumed, since a priori knowledge about the existence of an inhomogeneous distribution is usually not available. Nevertheless, the correction resulted in a correct estimate of the local channel density (Fig. 9 *B*) and retrieval of the correct kinetics as predicted by the spatial (Fig. 5) and temporal (Fig. 6) resolutions of the algorithm. The correction was successful for all tested locations; the conductance density slope along the apical dendrite was accurately retrieved (Fig. 9 *B*, *inverted triangles*). Results of this and of the correction of both a steeper (*solid circles*) and shallower (*triangles*) upwards gradients are summarized in Fig. 9 *B*. A decreasing gradient was also accurately extracted (Fig. 9 *C*).

## Dendritic recordings

All our simulations were performed under the assumption of a negligible series resistance. However, experimentally reached series resistances are at least several M$\Omega$, especially for dendritic recordings that can easily be above 20 M$\Omega$ (Stuart and Spruston, 1995; Stuart and Sakmann, 1994). The current injected by the voltage-clamp amplifier results in a voltage drop across the series resistance generated in the whole-cell configuration. Therefore, the voltage reported by most single-electrode voltage-clamp amplifiers is not correct (Armstrong and Gilly, 1992). The bigger the current injected by the amplifier, the bigger will be the error due to the series resistance. Conventional series resistance compensation, a part of any modern patch-clamp amplifier, can reasonably compensate resistances of up to 20 M$\Omega$ if the series resistance is measured accurately. When recording from neurons, the large currents and the high series resistance will greatly increase the error, thus rendering the use of patch-clamp amplifiers impossible. In principle, series resistance problems could be overcome by discontinuous voltage-clamp amplifiers. In these amplifiers, the current is injected for short durations followed by periods during which the voltage is recorded. Since the voltage is recorded during a time in which there is no current flowing across the series resistance, it is a true recording of the membrane potential. When this cycle is repeated at a high enough frequency, it is possible to voltage-clamp a cell even in the presence of a relatively high series resistance. However, application of such amplifiers to dendrites is not trivial because of the many membrane time constants inherent to neurons (Major, 1993; Wilson and Park, 1989). Furthermore, the existing discontinuous voltage-clamp amplifiers cannot cycle fast enough to accurately follow fast and large conductance changes. Therefore, the current method of choice for implementing our correction algorithm is the two-electrode voltage clamp. In this method, one electrode injects current while the other records the voltage. Both electrodes have series resistance due to the whole-cell configuration. However, since no current is injected via the voltage-sensing electrode, it is reporting the correct membrane potential. Furthermore, this technique can be tuned to follow very fast and large changes in membrane current.

To comply with the assumptions made while developing the correction algorithm, the morphology of the neuron and the passive parameters were determined as detailed in the methods. To isolate only $K^+$ currents, we blocked voltage-gated $Na^+$ channels with 1 $\mu$M TTX, voltage-gated $Ca^{2+}$ channels by complete substitution of the $Ca^{2+}$ in the bath with $Co^{2+}$, and $I_h$ with 30 $\mu$M of ZD2788. Two simultaneous whole-cell dendritic recordings were established at an in-

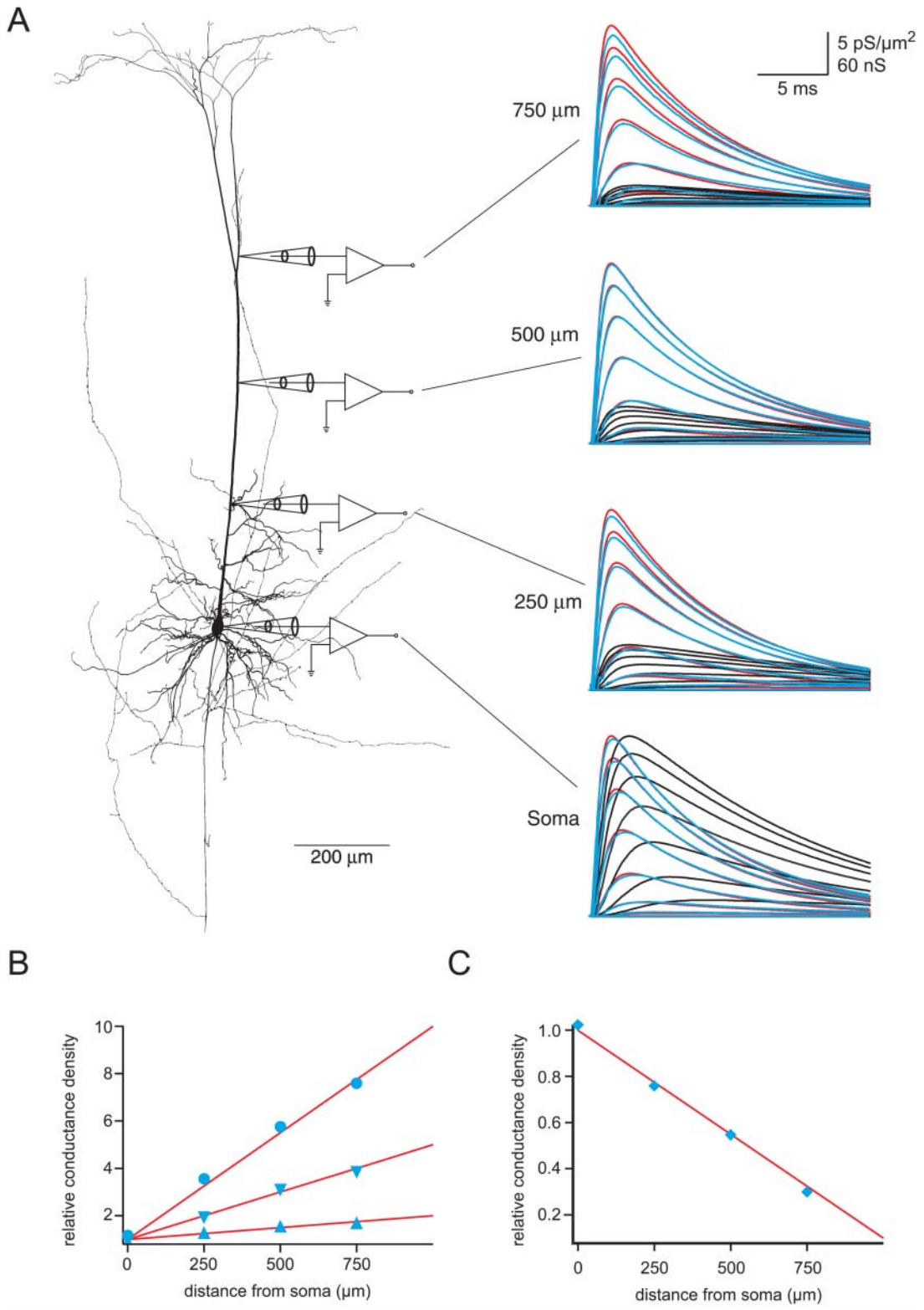


FIGURE 9 Space-clamp errors and correction of dendritic and somatic recordings of potassium channels. (*A*) The $K_{fast}$ channel with a homogenous density of 30 pS/$\mu$m$^2$ was inserted into a partially reconstructed morphology of a layer 5 neocortical pyramidal neuron (*left panel*). Voltage-clamp experiments were simulated at 0 $\mu$m, 250 $\mu$m, 500 $\mu$m, and 750 $\mu$m from the middle of the soma. The leak-subtracted and converted current recordings (*black lines*) and the corrected conductances (*blue lines*) are shown in the right panel. For comparison, the red lines indicate the true conductance kinetics and densities for the given positions. Scale bars apply to the uncorrected conductance (conductance in nS) and to the corrected and original kinetics (conductance density in pS/$\mu$m$^2$). (*B*) The reconstructed layer 5 pyramidal cell from *A* was equipped with a homogenous density of $K_{fast}$ ($g_{max}$ = 10 pS/$\mu$m$^2$) throughout the soma, the partially

terelectrode distance of 30–40 $\mu$m. Under these conditions it was possible to record $K^+$ currents from the dendrites of L5 neocortical pyramidal neurons. Fig. 10 *A* displays the schematic representation of the two-electrode voltage-clamp circuit with the current-injecting electrode at 220 $\mu$m and the voltage-sensing electrode at 180 $\mu$m measured from the center of the soma. The distorted currents, recorded voltage, and corrected conductance density are shown alongside the neuron (Fig. 10 *B*). Due to the initial overshoot of the potential (Fig. 10 *B*), the activation time course of the current was distorted and therefore not analyzed. The decay of the corrected conductance density was faster than the distorted currents as expected from our simulations. The correction clearly revealed a biexponential decay of the conductance density that was obscured in the distorted currents. This biexponential decay is probably the manifestation of the fast inactivating and slow inactivating $K^+$ conductances that are known to be present in the dendrites of layer 5 neocortical pyramidal neurons (Bekkers, 2000; Korngreen and Sakmann, 2000). The steady-state activation curve of the distorted conductances, calculated by dividing the distorted currents by the driving force, could be fitted to a Boltzmann function to obtain a $V_{1/2} = 27$ mV and $k = 22$ mV (average of 21 $\pm$ 3 mV and 17 $\pm$ 2 mV, $n = 3$). After correction, these parameters had values of $V_{1/2} = 18$ mV and $k = 16$ mV (average of 17 $\pm$ 2 mV and 14 $\pm$ 1 mV, $n = 3$). The corrected slope factor was not different ($P > 0.1$, ANOVA) from that obtained using somatic nucleated patches (12 $\pm$ 1 mV, $n = 6$) (Korngreen and Sakmann, 2000). The $V_{1/2}$, after correction for a liquid junction potential of 12 mV, was significantly different ($P < 0.05$, ANOVA) from the published value ($-1$ $\pm$ 2 mV, $n = 6$) (Korngreen and Sakmann, 2000).

## DISCUSSION

Space-clamp errors render proper analysis of ionic currents impossible in any branched or elongated structure. Here we present an algorithm (Fig. 3) that accurately extracts channel properties from distorted recordings (Figs. 4–9). Counterintuitively, the lack of space clamp offers the opportunity to obtain very local information about potassium-channel kinetics and densities (Fig. 5 and 9). The correction algorithm was not sensitive to added noise or to errors in passive membrane parameters (Fig. 7). Up until now, while performing voltage clamp in neurons, extreme measures were taken to increase the voltage control over a membrane area (Augustine et al., 1985). Such measures essentially flatten the voltage attenuation from the point of the clamp, thus reducing the error in the voltage. However, this only applies to structures with relatively short dendritic trees. Here we demonstrate that our algorithm performs best in the almost complete absence of space clamp. Since voltage attenuation upon channel activation is much narrower than in the well-studied passive case, the region that significantly influences the clamp current is limited to a narrow region around the electrode (''poor space clamp''). Thus, any method for estimation of membrane conductances will retrieve an averaged conductance only over this region, enabling high spatial resolution for poorly space-clamped structures (a small active $\lambda$; Fig. 5). The same principle applies to the temporal domain as follows. Many channel kinetics are slow compared to the membrane time constant for activated conductances (that is again much smaller than the well-known passive membrane time constant), therefore facilitating adaptation of our correction algorithm for the study of channel kinetics (Fig. 6).

With simplified channel models, which are described by only four parameters (three parameters for the activation curve in steady state and one voltage-invariant activation time constant), the correction algorithm accurately retrieved the entire channel model. Limitations of the algorithm were addressed by varying the four parameters (Figs. 4 and 6). Channels with a steep steady-state activation curve (inverse slope of the Boltzmann curve, $k \leq 4$ mV) could not be fully corrected due to the finite step size of the linear interpolation. Similarly, with very fast channel activation times ($\tau_{\text{channel}} \ll \tau_{\text{active}}$) a poorer correction was achieved, since essentially no kinetic model was assumed. Although these two difficulties are not a major concern in realistic channel models, they could be accounted for by including a priori assumptions about the activation curve or underlying channel kinetics. However, such assumptions substantially reduce the generality of the correction approach. Other problems, such as decreases in correction accuracy with decreasing $V_{1/2}$ of the Boltzmann activation curve, can be overcome by minor modifications of the algorithm, such as omission of the assumption of no channel activation at rest.

Correct implementation of the algorithm requires determination of both the morphology and passive parameters of the structure being studied. Given enough reconstructions, implementation might be simplified by building a canonical view of the specific neuron to obtain at least a first-order correction at a much reduced computation time, especially since the correction is sensitive primarily to local morpho-

reconstructed axon, and basal dendrites, and with a linearly increasing gradient along the apical dendrite (up to 50 pS/$\mu$m$^2$ at 1000 $\mu$m away from the soma). Correction was performed without any a priori knowledge of the gradient. The local recording was corrected with the underlying assumption of a homogenous distribution of a potassium conductance (*inverted triangles*). This procedure was repeated on a cell prepared with gradients of different steepness and sign: 20 pS/$\mu$m$^2$ (soma) to 40 pS/$\mu$m$^2$ (1000 $\mu$m distance), *triangles*; 7 pS/$\mu$m$^2$ to 70 pS/$\mu$m$^2$, *solid circles*; and (*C*) 70 pS/$\mu$m$^2$ down to 7 pS/$\mu$m$^2$, *solid diamonds*. Peak conductance densities were calculated and fitted with a Boltzmann function: $g/g_{\max} = (1/(1 + e^{-(V-V_{1/2})/k}))^n$, where $g/g_{\max}$ is the conductance normalized to its maximal value, $V$ is membrane potential, $V_{1/2}$ is the voltage at which half of the ''gates'' of all channels are in the open configuration, and $k$ is the slope factor. $g_{\max}$ was normalized to the true somatic value for display purposes.

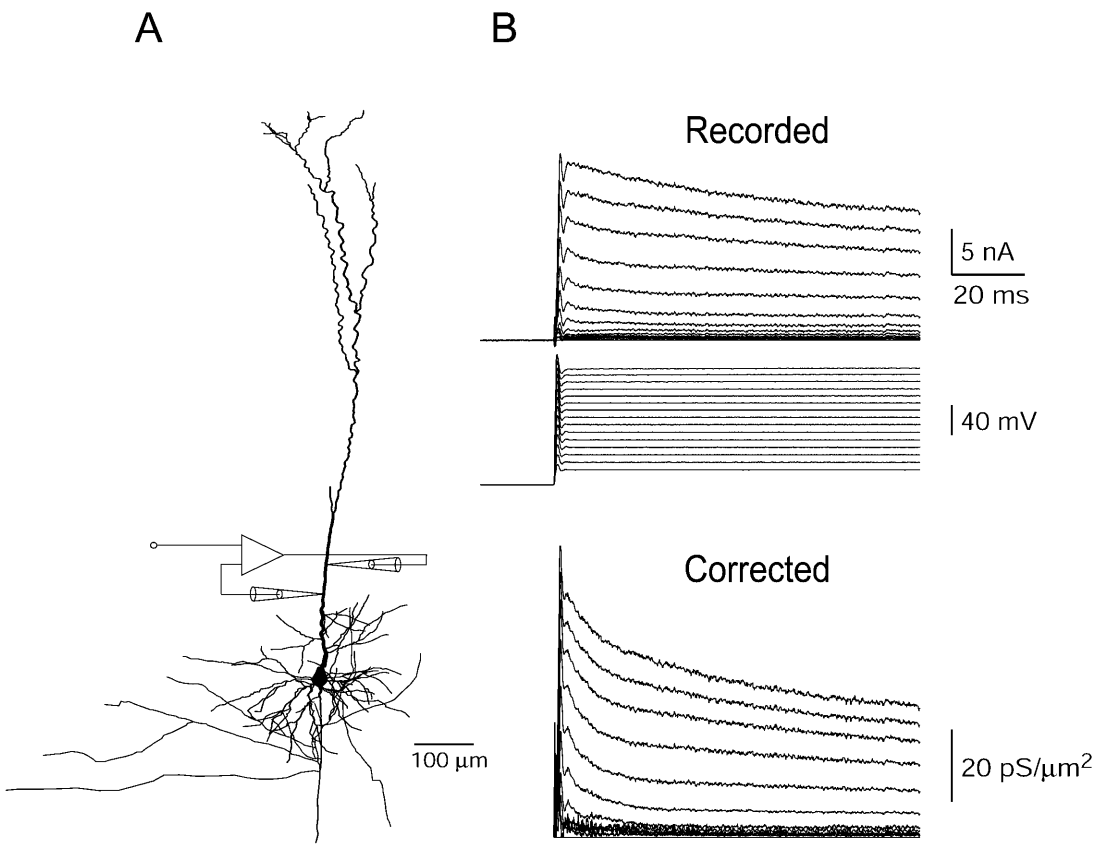


FIGURE 10 Dendritic two-electrode voltage-clamp recording of $K^+$ currents. (*A*) The schematic representation of a two-electrode voltage-clamp circuit is shown at the recording site on the dendrite of the reconstructed neuron. (*B*) The distorted currents, membrane voltage, and corrected conductance density are shown from top to bottom. The data was sampled at 10 kHz and filtered at 5 kHz. Both the current-injecting and the voltage-sensing electrodes had series resistances of 25 MΩ. The passive parameters determined as detailed in Methods were $R_i = 90\ \Omega$cm, $R_m = 51{,}000\ \Omega$cm$^2$, and $C_m = 1.1\ \mu$F cm$^{-2}$.

logical features (Fig. 5). The effects of changes in distal morphology are in general minor (as partially discussed in the Appendix). Simplifying distant parts of the dendritic tree could thus substantially both ease and speed up the reconstruction process and enhance computational efficacy. This becomes important not mainly for the demonstration of the basic principles (that are assessed in a cylinder model) but for the application to various complex dendritic trees. We observed significant errors in the correction only if the reconstruction became poor in regions closer than ~200 $\mu$m to the recording site on the dendrite (data not shown). For experimental implementability it could therefore be useful to extract the local dendritic morphology during the experiment (e.g., by imaging methods) and combine it with a simple generic cell morphological model to result in a quick semi-online correction. In a post hoc analysis, a slightly more detailed morphological measurement might already be sufficient. This can always be tested by further simplifying the morphology and testing whether any significant changes in the corrected conductance values occur. If this is not the case, it is safe to assume that the morphological reconstruction is sufficient.

Of concern also is the accuracy of the passive membrane parameters ($R_m$, $R_i$, and $C_m$). A 10–20% error in the passive parameters did not significantly affect the final outcome (Fig. 7). The passive parameters of a given neuron can be estimated with reasonable accuracy once its morphology is known (Clements and Redman, 1989; Major et al., 1994; Roth and Häusser 2001; Stuart and Spruston, 1998). This requires an additional pulse protocol in current-clamp mode, before the voltage-clamp experiment, and a full reconstruction of the neuron afterward (Clements and Redman, 1989; Major et al., 1994; Roth and Häusser 2001; Stuart and Spruston, 1998). As the neuron usually is to be reconstructed for use in the correction algorithm, only additional pulse protocols in current clamp need to be performed. Previously, many recorded sweeps were claimed to be needed to obtain a sufficiently accurate estimate of the passive parameters (Major et al., 1994). However, using two electrodes to record such sweeps (Roth and Häusser, 2001; Stuart and Spruston, 1998) greatly reduces the number of sweeps required. Thus, obtaining the passive parameters for each neuron before starting the voltage-clamp experiment does not require more than an additional 5–10 min. Another advantage of the two-electrode voltage clamp is that the series resistance of the two electrodes can be considerably higher than the one required

for the accurate application of a single-electrode voltage clamp. We were able to voltage-clamp dendrites even when both electrodes had series resistance of 25–30 MΩ. Although more recordings are required to establish the full kinetic and density profile of the $K^+$ conductances along the apical dendrite of L5 pyramidal neurons, it is clear that the correction algorithm was able to correct currents recorded in the absence of space clamp.

Here, we present an algorithm that extracts only activation curves of single or mixtures of potassium channels. Much more information can be obtained from the voltage-clamp technique with carefully planned voltage protocols. Using the correction of the activation curve as a cornerstone, inactivation properties and activation kinetics can also be corrected (M.H., A.T.S., B.S., and A.K., in preparation). We applied the algorithm to a variety of potassium channels. As outlined in the text, the algorithm works best for nonregenerative currents. Thus, under physiological conditions, the algorithm can be applied to potassium channels, as shown in Fig. 10, and chloride channels, as well as, in the opposite direction, to $I_h$ and inward rectifier channels. Sodium and calcium channels, the two other important classes of voltage-gated ion channels in neurons would, due to the lack of space clamp, generate regenerative events, which will be observed as ''voltage escapes'' to the recording electrode. Such events do not comply with the basic assumption of the correction algorithm that the membrane potential does not exceed the clamp voltage anywhere in the entire structure. This problem might be overcome by designing an experiment in which the probability of regenerative events is low.

The principle we developed for the correction of currents from voltage-gated channels could in general be applied to estimate the conductance density of ligand-gated channels and that of synaptic currents as well. However, several problems need to be addressed first. It is possible to design an experiment in which a puff of a neurotransmitter will be applied to the dendrite at the location of a voltage-clamp electrode. This experiment will suffer from the lack of knowledge of the membrane area onto which the neurotransmitter was applied because of the dense structure of the brain slice and the speed of the perfusion system. It is important to stress that the neurotransmitter must be applied to the location of the voltage clamp. Application to a site on the dendrite farther away from the electrode introduces more free parameters to be estimated by the algorithm: knowledge of the site of application and the distance to the recording, active contributions to the signal propagation by voltage-gated channels, and nonuniformity of the passive parameters between the application site and the recording electrode. Above all, at a site of a remote application, there is virtually no control of the membrane potential by the voltage-clamp electrode. Thus, we cannot use the same iterative approach as detailed in this paper. This problem is worse for the correction of synaptic currents. The release of neurotransmitter is variable and dependent on the properties of the presynaptic terminal. Thus, we have very little control over the amount of neurotransmitter released and over the voltage at both pre- and postsynaptic terminals. To allow the correcting of space-clamp distortions of synaptic currents, it may be possible to combine our approach with new ways of influencing the membrane potential at the synapse or measuring the membrane potential at multiple positions to facilitate estimates regarding the signal propagation.

Many voltage-clamp recordings are limited by the absence of proper space clamp. Even neurons with relatively short dendrites will produce erroneous current recordings due to voltage drop in the dendrites. Here we present an algorithm to correct for such distortions with the aid of computer-simulated experiments, and described its application to L5 pyramidal neurons. Since the functionality of this correction algorithm does not depend on specific properties of the studied structure, it can be used to analyze voltage-clamp recordings in any type of nonisopotential cell or fiber.

## APPENDIX

### The reverse problem: monotonicity of the clamp current-conductance relation

With complete knowledge of conductance kinetics and distributions, cable theory allows calculation of clamp currents from the conductance properties. As outlined in the Results section, in voltage-clamp experiments one is faced with the far more difficult reverse problem: to determine the conductance distribution and kinetics from the clamp-current recording. The algorithm described above breaks down this multiparameter problem into several one-parameter problems, each linking one current recording (e.g., the clamp current $I$ in the steady state of a voltage-clamp experiment to −40 mV) to a single yet unknown conductance value (the steady-state conductance $g$ for voltages $-50\ \text{mV} < V \leq -40\ \text{mV}$). The reverse problem is thus to invert the relation $I(g)$ to determine the conductance $g_0$ that matches the experimentally measured clamp current $I_{exp} = I(g_0)$. A sufficient and in most cases essential prerequisite for solving the reverse problem is therefore monotonicity of this clamp current-conductance relation. However, an increase in the membrane conductance results in a narrowing of the voltage profile. Therefore only a smaller region contributes substantially to the clamp current. Whether the increase in the membrane conductance is not usually overcompensated by the decrease in the activated region due to the narrowing voltage profile must hence be examined.

In the following, we analytically examine the clamp current-conductance relation in several scenarios. In the general case of an arbitrary voltage-dependent conductance $g(V)$ a complete analytic solution is impossible to obtain. In a simplified situation with a very simple voltage dependence $g(V) = g_0$ (for $V < V_0$) and $g(V) = g_1$ (for $V \geq V_0$), a complete analytical solution can be derived as outlined in the first paragraph. For more complex voltage dependencies, this is not possible any more. Thus, we describe approximations of the clamp current-conductance relation that allow to qualitatively predict its overall shape (and thus its monotonicity). These solutions are then compared to the exact analytical solution and numerical calculations.

Let us consider the steady-state situation in an infinite cylinder (equipped with a voltage-dependent conductance density $g$ measured per membrane area) that is voltage-clamped to $V_{clamp}$ at position $x = 0$ (Fig. 11 *A*). The voltage dependence of $g$ to be $g(V) = g_0$ (for $V < V_0$) and $g(V) = g_1$ (for $V \geq V_0$; higher voltages do not occur in the clamp experiment: $V \leq V_{clamp}$ throughout the cylinder as reversal potentials are assumed to be hyperpolarized (as described in the Results section)), as

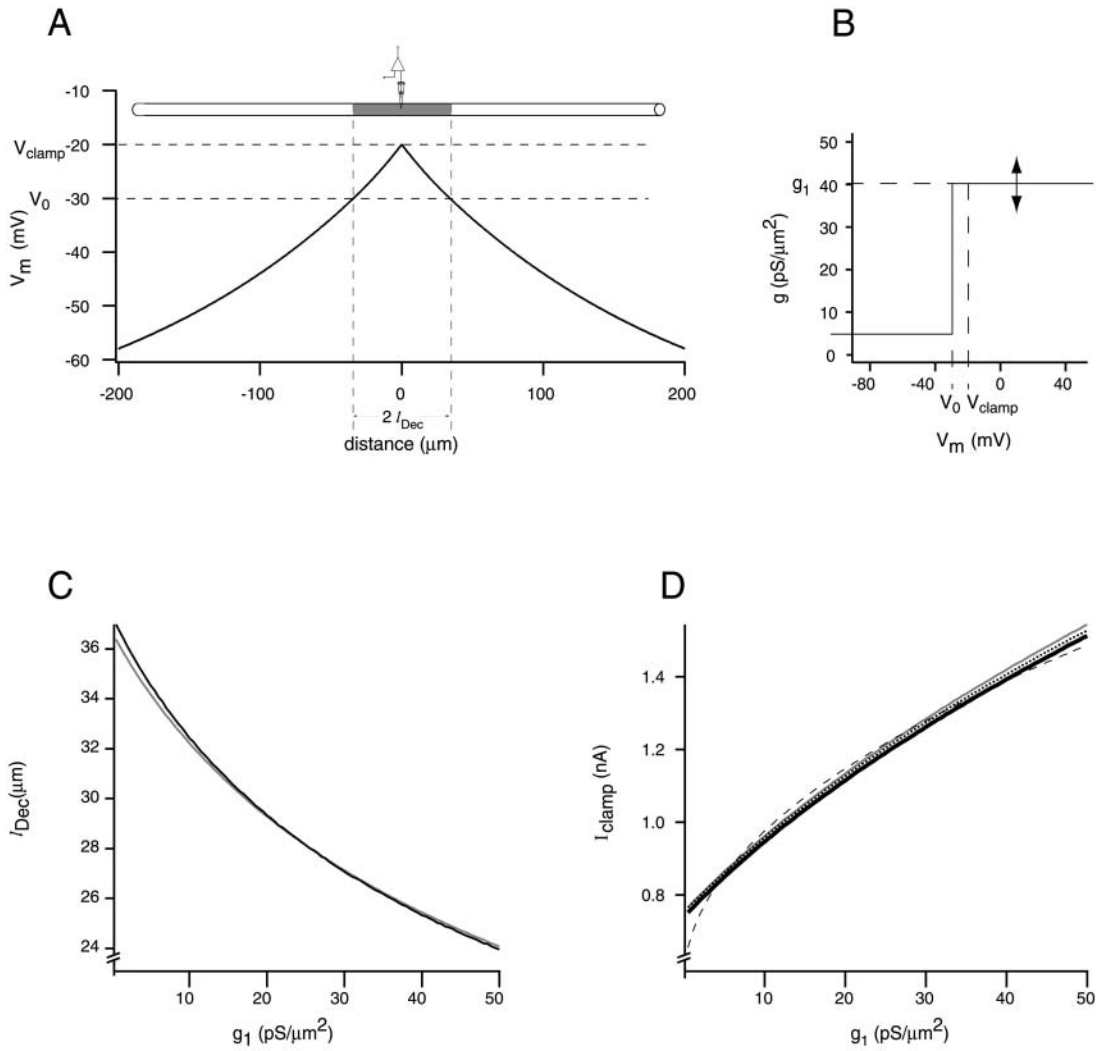


FIGURE 11 Monotonicity of the clamp current-conductance relation. (*A*) A voltage-clamp experiment was simulated in a long unbranched cable as for Fig. 2. Outer regions of the cylinder are clipped for displaying purposes. The voltage attenuation in steady state is shown for a simulated voltage clamp to −20 mV in the middle of the cable. $l_{Dec}$, the decreasing length, is the length for which the voltage drops from −20 to −30 mV. (*B*) The voltage-dependent membrane conductance was time-independent, $g_0 = 5\ \mathrm{pS}/\mu\mathrm{m}^2$ for voltages $V < -30$ mV, and $g_1 = 40\ \mathrm{pS}/\mu\mathrm{m}^2$ for voltages $V \geq -30$ mV. (*C*) Dependence of the decreasing length $l_{Dec}$ on the membrane conductance $g_1$. (*D*) Dependence of the clamp current on the membrane conductance $g_1$. The calculations underlying the analytical (*gray* and *dotted* lines) and approximate (*dashed line*) traces in *C* and *D* are detailed in the Appendix. Simulation results in *C* and *D* are indicated by black lines.

shown in Fig. 11 *B*. The cylinder can be divided into three parts: one finite cylinder with length $2l_{Dec}$ around the voltage clamp (*gray* in Fig. 11 *A*) and two semi-infinite cylinders (*white*). $l_{Dec}$ indicates the length over which the voltage attenuates from the clamp voltage $V_{clamp}$ to the voltage $V_0$. Therefore, in the gray cylinder, the membrane voltage is larger than $V_0$ at each position. With the voltage-dependent conductance defined as above, i.e., constant for $V \geq V_0$, this results in an ohmic membrane conductance $g = g_1$ for the gray cylinder. For the white cylinders, $V < V_0$, therefore $g = g_0$. All the properties of the white cylinders are independent of $g_1$, since changes in $g_1$ only influence $l_{Dec}$, not the length nor membrane properties of the white cylinders (at this point the assumption of an infinite cylinder substantially simplifies the calculation).

## The analytical solution

For a finite cylinder with an ohmic membrane conductance and a terminating resistance $R_L$ (Fig. 11, $R_L$ being the known input resistance of the semi-infinite cylinder (*white*) with membrane conductance $g_0$), the input resistance is $G_{inp} = 2G_\infty(R_\infty + R_L \tanh(L))/(R_L + R_\infty \tanh(L))$ (for derivation see e.g., Koch, 1999, chapter 2.2, page 37), with $L = l_{Dec}/\lambda_{gray} = 2l_{Dec}\sqrt{R_i g_1/d}$ and $G_\infty = 1/R_\infty = \sqrt{g_1/R_i}\pi d^{3/2}/2$ being the input conductance of a semi-infinite cylinder with the membrane properties of the gray cylinder. $R_i$ is the morphology-independent, specific axial resistance of the cylinder; $d$ its diameter. The clamp current can then be calculated as

$$I_{clamp} = (V - E_k) \cdot G_{inp} = 2(V - E_k)G_\infty \frac{R_\infty + R_L \tanh(L)}{R_L + R_\infty \tanh(L)}, \quad (1)$$

which is depicted in Fig. 11 *D* as a dotted line. No free parameters needed to be fitted.

## Approximate solutions

The clamp current required can—in very general terms—be written as

$$I_{\text{clamp}} = I_{\text{white}} + I_{\text{gray}}, \tag{2}$$

$I_{\text{white}}$ being the contribution of the white cylinders (independent of $g_1$) and $I_{\text{gray}}$ being the contribution of the gray cylinder that is dependent on $g_1$. This holds true for both the situation described above ($g = const$ in the white cylinder) and for an arbitrary voltage dependence $g(V < V_0)$. For a first approximation, a rough estimate of the $g_1$-dependence of $I_{\text{gray}}$ can be calculated from the membrane conductance and the membrane area as $I_{\text{gray}} \approx c\ 2l_{\text{Dec}}g_1$. The constant $c$ could be derived from the driving force and the cylinder diameter. What is important for the estimate is, however, that $c$ is almost independent of $g_1$. With increasing $g_1$, the voltage profile narrows, thus resulting in a smaller $l_{\text{Dec}}$. To assess the question, whether the current-conductance relation is monotonic, in this first estimate it remains to be shown that the decrease in $l_{\text{Dec}}$ does not overcompensate the increase in $g_1$. With the intrinsic length scale of the gray cylinder being $\lambda_{\text{gray}}$, a first estimate for $l_{\text{Dec}}$ is $l_{\text{dec}} \propto \lambda_{\text{gray}} \propto 1/\sqrt{g_1}$ and therefore $I_{\text{gray}} \approx c \cdot (1/\sqrt{g_1}) \cdot g_1 = c\sqrt{g_1}$. Substitution of this approximation into Eq. 2 yields a first approximation for the clamp current

$$I_{\text{clamp}} = I_{\text{white}} + c\sqrt{g_1}. \tag{3}$$

Since $I_{\text{white}}$ and $c$ are (almost) $g_1$-independent fit parameters, it becomes evident, that $I_{\text{clamp}}$ is indeed monotonic, and a first approximation (*dashed line* in Fig. 11 *D*) of the actual (calculated in simulation, *black line*) clamp current-conductance relation can be obtained.

As outlined above, for a more general conductance ($g(V)$ is arbitrary for $V < V_0$ and $g(V) = g_1$ for $V_{\text{clamp}} \geq V \geq V_0$), the only difference to the step conductance is in the contribution of the white cylinders. Therefore, the above argument still holds for arbitrary voltage dependence for voltages $V < V_0$, with the only change being in the parameters $I_{\text{white}}$ and $c$.

To more accurately assess the validity of the $g_1$-dependence of $l_{\text{Dec}}$, it was calculated analytically for the step-conductance as follows (depicted in Fig. 11 *C*): From the general voltage distribution $V(X < L) = \alpha\cosh(L - X) + \beta\sinh(L - X)$, the boundary condition for the gray cylinder $V_o/R_L = -(1/r_a\lambda)(dV/dX)|_{X=L}$ ($r_a$ indicates the axial resistance per unit length, see also Koch, 1999, pages 33–37), and the boundary condition $V(L) = V_0$, one obtains $V_o/R_L = (1/r_a\lambda)(V_{\text{clamp}} - V_o\cosh(L))/\sinh(L)$. Since $L = l_{\text{Dec}}/\lambda \ll 1$, a Taylor expansion for the hyperbolic functions yields a square equation for $l_{\text{Dec}}$, and finally $l_{\text{Dec}} = -\kappa_1/g_1 + \sqrt{(\kappa_1^2/g_1^2) + (\kappa_2/g_1)}$, with $\kappa_1 = 1/2\sqrt{g_0 d/R_i}$ and $\kappa_2 = ((V_{\text{clamp}}/V_0) - 1)(d/2R_i)$.

The clamp current can then be approximated by:

$$I_{\text{clamp}} = 2\left((V_0 - E_k)\frac{1}{R_L} + \frac{V_0 + V_{\text{clamp}}}{2}\pi d l_{\text{Dec}} g_1\right) \tag{4}$$

as shown in gray in Fig. 11 *D*.

## Effects of distal membrane properties on clamp-current recordings

The sensitivity of conductance estimates from the correction algorithm to changes in distal membrane properties (which reflects incomplete knowledge about the spatial distribution of e.g., passive properties) was assessed by studying the dependence of the clamp-current recordings on the membrane conductances in regions distal to the recording electrodes (Fig. 5). For this purpose, an infinite cylinder was divided into three regions: a middle region around the voltage-clamp electrode with a length of $2l$ and an ohmic membrane conductance $g_M$ (Fig. 5 *A*, *gray*), and two semi-infinite cylinders with ohmic membrane conductances $g_D$ (Fig. 5 *A*, *white*). The clamp current was calculated according to Eq. 1

$$I_{\text{clamp},g_D,g_M} = 2(V - E_k)G_\infty \frac{R_{\infty,\text{middle}} + R_{\text{side}}\tanh(l/\lambda_{\text{middle}})}{R_{\text{side}} + R_{\infty,\text{middle}}\tanh(l/\lambda_{\text{middle}})},$$

$\lambda_{\text{middle}}$, $R_{\infty,\text{middle}}$, $G_\infty$, and $R_{\text{side}}$ being the space constant of the middle cylinder, the input resistance, input conductance of a semi-infinite cylinder with the membrane conductance $g_M$, and the input resistance of the white semi-infinite cylinder, respectively. The relative change in the clamp current $(I_{\text{clamp}}(0.5g_D, g_M) - I_{\text{clamp}}(g_D, g_M))/I_{\text{clamp}}(g_D, g_M)$ was calculated as a function of the relative input resistances $R_{\text{side}}/R_{\infty,\text{middle}} = \sqrt{g_M/g_D}$ of the cylinders indicating the sensitivity of the clamp-current recording to changes in distal membrane properties.

## Piecewise linear conductance models

To increase the accuracy of the conductance calculations, the staircase conductance approach was changed to a piecewise linear conductance model. Again, in the first step of the correction algorithm, the conductance $g_1 = g(-70\text{ mV})$ was estimated. To achieve this, the voltage-clamp experiment stepping to $-70$ mV was simulated as described above with the only difference that the conductance model was $g(V) = 0$ ($V < -80$ mV) and $g(V) = (V + 80\,\text{mV})/10\,\text{mV} \cdot g_1$ ($-80$ mV $< V \leq -70$ mV, higher voltages do not occur). This resulted in a conductance-voltage relation that is continuous and piecewise linear. The conductance $g_1$ (and thus the slope of the conductance voltage relation for $-80\text{ mV} < V \leq -70$ mV) was varied to minimize the clamp current difference. Similarly, at higher voltages $V_n$, the conductance for $V_n - 10\text{ mV} < V \leq V_n$ was assumed to be linear across this voltage region. From the last correction step, $g_{n-1} = g(V_n - 10\text{ mV})$ was known. Thus the conductance for the voltage region of interest can be written as $g(V) = g_{n-1} + (V - (V_n - 10\,\text{mV}))/10\,\text{mV} \cdot (g_n - g_{n-1})$. During the fitting procedure, $g_n$ (and thus the slope of the conductance-voltage relation for voltages $V$ with $V_n - 10\text{ mV} < V \leq V_n$) is varied to match the clamp currents.

## Potassium-channel models

For all realistic channel models used, potassium currents were calculated as $I_K = g_{\max}a^x b(v - E)$, where $g_{\max}$ is the local conductance density; $a$ and $b$ indicate the activation particle with an $x$-order kinetic and the inactivation particle, respectively; $v$ is the local membrane voltage; and $E$ the potassium reversal potential. Activation and inactivation variables are expressed in terms of a steady-state value $a_\infty(v)$ and a time constant $\tau_a(v)$. For $K_v$, $K_m$, $K_{\text{fast}}$, and the activation of $K_{\text{slow}}$, steady-state value and time constant were determined as $a_\infty = \alpha/(\alpha + \beta)$ and $\tau_a = 1/(\alpha + \beta)$. The rate functions $\alpha$ and $\beta$ were as follows ($v$ in mV, $\tau$ in ms, and $\alpha$ and $\beta$ in $\text{ms}^{-1}$):

Delayed rectifier $K^+$ channel $K_v$ (Mainen et al., 1995):

$$(\text{no inactivation},\ x = 1);\quad \alpha = 0.02\frac{(v - 25)}{1 - e^{-(v-25)/9}};$$
$$\beta = -0.002\frac{(v - 25)}{1 - e^{(v-25)/9}}.$$

Muscarinic $K^+$ channel $K_m$ (Mainen et al., 1995):

$$(\text{no inactivation},\ x = 1);\quad \alpha = 0.001\frac{(v + 30)}{1 - e^{-(v+30)/9}};$$
$$\beta = -0.001\frac{(v + 30)}{1 - e^{(v+30)/9}}.$$

Fast inactivating $K^+$ channel from neocortical neurons $K_{fast}$ (Korngreen and Sakmann, 2000):

$$\text{Activation } (x = 4)\ \alpha = \frac{3.4}{1 + e^{-(v-10)/30}};$$
$$\beta = 0.7\, e^{v-6/180} - 0.45.$$

$$\text{Inactivation } \alpha = 0.0001\, e(-0.06v);$$
$$\beta = \frac{0.12}{1 + e(-(v + 50)/8)} + 0.002.$$

Slow inactivating $K^+$ channel from neocortical neurons $K_{slow}$ (Korngreen and Sakmann, 2000):

$$\text{Activation } (x = 2)\ \alpha = 0.0052\frac{v - 11.1}{1 - e^{-(v-11.1)/13.1}};$$
$$\beta = 0.01938\ e^{-(v+1.27)/71} - 0.0053.$$

Inactivation was described as $b(t, v) = c_1(v)b_1(t, v) + c_2(v)b_2(t, v)$ with first order rate equations for $b_1$ and $b_2$.

$$b_{1\infty} = b_{2\infty} = \frac{1}{1 + e^{(v+58)/11}};$$
$$\tau_{b1} = 360 + (1010 + 23.7(v + 54))e^{-((v+75)/48)^2};$$
$$\tau_{b2} = 3330 - 4v;$$
$$c_2 = \begin{cases} 1 & v > -10 \\ 0 & v \le -10 \end{cases}; \quad c_1 = 1 - 0.55c_2.$$

Fast inactivating $K^+$ channel from hippocampal neurons $K_a$ (Hoffman et al., 1997):

$$\text{Activation } (x = 1):$$
$$a_\infty = 1/(1 + e^{-0.001(1.5-(39(v-11)/(1+e^{(v+40)/5})))});$$
$$\tau_a = e^{-0.0015-(21.5(v-11)/(1+e^{(v+40)/5}))} \cdot a_\infty(v).$$

$$\text{Inactivation}: \ b_\infty = \frac{1}{1 + e^{0.117(v+56)}}; \quad \tau_b = 0.26(v + 50).$$

We thank Dr. Sebastian Bergling for help with the construction of the $K_{slow}$ and $K_{fast}$ MOD files; Drs. Nathan Urban, Dirk Feldmeyer, Troy Margrie, Fritjof Helmchen, and in particular Arnd Roth for helpful discussions and critical reading of the manuscript; and Klaus Bauer and Klaus Rohm for maintaining the computer environment that enabled performance of the required calculations.

## REFERENCES

Adrian, R. H., W. K. Chandler, and A. L. Hodgkin. 1970. Voltage clamp experiments in striated muscle fibers. *J. Physiol.* 208:607–644.

Armstrong, C. M., and W. F. Gilly. 1992. Access resistance and space clamp problems associated with whole-cell patch clamping. *Methods Enzymol.* 207:100–122.

Augustine, G. J., M. P. Charlton, and S. J. Smith. 1985. Calcium entry and transmitter release at voltage-clamped nerve terminals of squid. *J. Physiol.* 367:163–181.

Bekkers, J. M. 2000. Distribution and activation of voltage-gated potassium channels in cell-attached and outside-out patches from large layer 5 cortical pyramidal neurons of the rat. *J. Physiol.* 525:611–620.

Benardo, L. S., L. M. Masukawa, and D. A. Prince. 1982. Electrophysiology of isolated hippocampal pyramidal dendrites. *J. Neurosci.* 2:1614–1622.

Bischofberger, J., and P. Jonas. 1997. Action potential propagation into the presynaptic dendrites of rat mitral cells. *J. Physiol.* 504:359–365.

Clements, J. D., and S. J. Redman. 1989. Cable properties of cat spinal motoneurones measured by combining voltage clamp, current clamp and intracellular staining. *J. Physiol.* 409:63–87.

Cole, K. S., and H. J. Curtis. 1941. Membrane potential of the squid giant axon during current flow. *J. Gen. Physiol.* 24:551–563.

Hines, M. L., and N. T. Carnevale. 1997. The NEURON simulation environment. *Neural Comput.* 9:1179–1209.

Hodgkin, A. L., and A. F. Huxley. 1952. A quantitative description of membrane current and its application to conduction and excitation in nerve. *J. Physiol.* 117:500–544.

Hoffman, D. A., J. C. Magee, C. M. Colbert, and D. Johnston. 1997. $K^+$ channel regulation of signal propagation in dendrites of hippocampal pyramidal neurons. *Nature.* 387:869–875.

Johnston, D., J. C. Magee, C. M. Colbert, and B. R. Cristie. 1996. Active properties of neuronal dendrites. *Annu. Rev. Neurosci.* 19:165–186.

Kavalali, E. T., M. Zhuo, H. Bito, and R. W. Tsien. 1997. Dendritic $Ca^{2+}$ channels characterized by recordings from isolated hippocampal dendritic segments. *Neuron.* 18:651–663.

Koch, C. 1999. Biophysics of Computation. Oxford University Press, Oxford.

Korngreen, A., and B. Sakmann. 2000. Voltage-gated $K^+$ channels in layer 5 neocortical pyramidal neurones from young rats: subtypes and gradients. *J. Physiol.* 525:621–639.

Larsson, H. P., S. J. Kleene, and H. Lecar. 1997. Noise analysis of ion channels in non-space-clamped cables: estimates of channel parameters in olfactory cilia. *Biophys. J.* 72:1193–1203.

Magee, J. C. 1999. Dendritic $I_h$ normalizes temporal summation in hippocampal CA1 neurons. *Nat. Neurosci.* 2:508–514.

Magee, J. C., and D. Johnston. 1995. Characterization of single voltage-gated $Na^+$ and $Ca^{2+}$ channels in apical dendrites of rat CA1 pyramidal neurons. *J. Physiol.* 487:67–90.

Mainen, Z. F., J. Joerges, J. R. Huguenard, and T. J. Sejnowski. 1995. A model of spike initiation in neocortical pyramidal neurons. *Neuron.* 15:1427–1439.

Major, G. 1993. Solutions for transients in arbitrarily branching cables: III. Voltage clamp problems. *Biophys. J.* 65:469–491.

Major, G., J. D. Evans, and J. J. Jack. 1993. Solutions for transients in arbitrarily branching cables: II. Voltage clamp theory. *Biophys. J.* 65: 450–468.

Major, G., A. U. Larkman, P. Jonas, B. Sakmann, and J. J. Jack. 1994. Detailed passive cable models of whole-cell recorded CA3 pyramidal neurons in rat hippocampal slices. *J. Neurosci.* 14:4613–4638.

Müller, W., and H. D. Lux. 1993. Analysis of voltage-dependent membrane currents in spatially extended neurons from point-clamp data. *J. Neurophysiol.* 69:241–247.

Nadeau, H., and H. A. Lester. 2000. Two-compartment model for whole-cell data analysis and transient compensation. *J. Neurosci. Meth.* 99: 25–35.

Press, W. H., S. A. Teukolsky, W. T. Vetterling, and B. P. Flannery. 1992. Numerical Recipes in C, the Art of Scientific Computing, 2nd ed. Cambridge University Press, Cambridge.

Rall, W. 1959. Branching dendritic trees and motorneuron membrane resistivity. *Experimental Neurobiology.* 1:491–527.

Rall, W., R. E. Burke, W. R. Holmes, J. J. Jack, S. J. Redman, and I. Segev. 1992. Matching dendritic neuron models to experimental data. *Physiol. Rev.* 72 (4 Suppl):S159–S186.

Rall, W., and I. Segev. 1985. Space clamp problems when voltage clamping branched neuron with intracellular microelectrodes. *In* Voltage and Patch Clamping with Microelectrodes. T. G. Smith, H. Lecar, S. J. Redman, and P. W. Gage, editors. 191–215.

Roth, A., and M. Häusser. 2001. Compartmental models of rat cerebellar Purkinje cells based on simultaneous somatic and dendritic patch-clamp recordings. *J. Physiol.* 535:445–472.

Spruston, N., D. B. Jaffe, S. H. Williams, and D. Johnston. 1993. Voltage- and space-clamp errors associated with the measurement of electrotonically remote synaptic events. *J. Neurophysiol.* 70:781–802.

Stuart, G., and N. Spruston. 1995. Probing dendritic function with patch pipettes. *Curr. Opin. Neurobiol.* 5:389–394.

Stuart, G., and N. Spruston. 1998. Determinants of voltage attenuation in neocortical pyramidal neuron dendrites. *J. Neurosci.* 18:3501–3510.

Stuart, G., N. Spruston, B. Sakmann, and M. Häusser. 1997. Action potential initiation and backpropagation in neurons of the mammalian CNS. *Trends Neurosci.* 20:125–131.

Stuart, G. J., H.-U. Dodt, and B. Sakmann. 1993. Patch-clamp recordings from the soma and dendrites of neurons in brain slices using infrared video microscopy. *Pflugers Arch.* 423:511–518.

Stuart, G. J., and B. Sakmann. 1994. Active propagation of somatic action potentials into neocortical pyramidal cell dendrites. *Nature.* 367:69–72.

Takigawa, T., and C. Alzheimer. 1999. G protein-activated inwardly rectifying $K^+$ (GIRK) currents in dendrites of rat neocortical pyramidal cells. *J. Physiol.* 517:385–390.

White, J. A., N. S. Sekar, and A. R. Kay. 1995. Errors in persistent inward currents generated by space-clamp errors: a modeling study. *J. Neurophysiol.* 73:2369–2377.

Wilson, C. J., and M. R. Park. 1989. Capacitance compensation and bridge balance adjustment in intracellular recording from dendritic neurons. *J. Neurosci. Meth.* 27:51–75.